

Bringing the Context Back into Object Recognition, Robustly

Klara Janouskova Cristian Gavrus Jiri Matas
 Visual Recognition Group, Czech Technical University in Prague
 {klara.janouskova, gavrucri, matas}@fel.cvut.cz

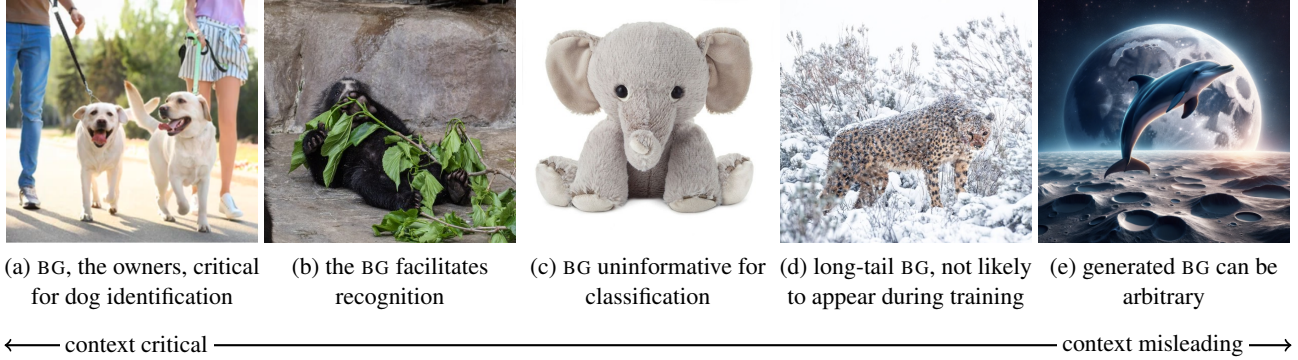


Figure 1. The complementarity of foreground (FG) and background (BG) in recognition. The standard approach, background suppression, makes correct identification in (a) nearly impossible, and difficult in (b); the spectacled bear is the most herbivorous of all bear species. On the other hand, rare backgrounds with possibly huge diversity hurt classification – (d) shows a cheetah after a snowfall in South Africa, not a snow leopard. In generated content (e), any FG can appear on any BG as in ChatGPT 4o’s response to “a dolphin on the moon”.

Abstract

In object recognition, both the subject of interest (referred to as foreground, FG, for simplicity) and its surrounding context (background, BG) may play an important role. However, standard supervised learning often leads to unintended over-reliance on the BG, limiting model robustness in real-world deployment settings. The problem is mainly addressed by suppressing the BG, sacrificing context information for improved generalization.

We propose “Localize to Recognize Robustly” ($L2R^2$), a novel recognition approach which exploits the benefits of context-aware classification while maintaining robustness to distribution shifts. $L2R^2$ leverages advances in zero-shot detection to localize the FG before recognition. It improves the performance of both standard recognition with supervised training, as well as multimodal zero-shot recognition with VLMs, while being robust to long-tail BGs and distribution shifts. The results confirm localization before recognition is possible for a wide range of datasets and they highlight the limits of object detection on others¹.

¹The code will be made publicly available on GitHub

1. Introduction

In standard object recognition, a neural network models the statistical distribution of the objects’ appearance in the training set. This approach has been highly successful in i.i.d. settings, particularly with moderate to large-scale training data.

As object recognition matured, analyses of its weaknesses [47, 59] revealed that supervised classifiers are particularly prone to unintended over-reliance on the background (BG). This seriously impacts model robustness in real-world deployment settings as BG shortcuts [15] perform well on training data but fail to generalize to BGs which are long-tail, i.e. rarely or never appearing in the training data, and to substantial BG distribution shifts, not an uncommon situation.

Recent methods address the problem by suppression of BG features. The methods can be broadly categorized into two groups: the first emphasizes FG features during training [2, 7, 11, 61] by exploiting segmentation masks (often ground truth) or saliency maps, the second alters the BG distribution [4, 16, 45, 55, 59] through image augmentation and generation techniques.

However, as Figure 1 illustrates, context may play a critical role in object recognition [1, 13, 35, 39, 50, 51, 64, 65].

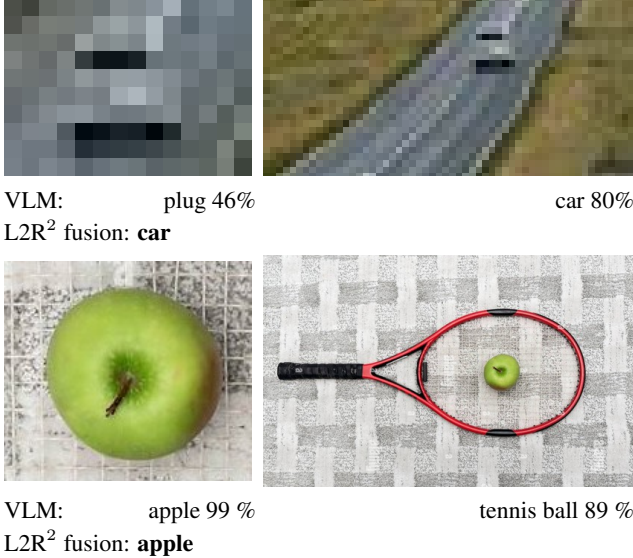


Figure 2. VLM (CLIP-B) – zero-shot recognition with ground truth prompts and selected distractors. In the top example, recognition fails on the foreground (left, crop of a tight object bounding box). In the bottom, it fails on the full image (right). The proposed L2R² fusion is correct both times.

Certain classes are difficult to recognize from FG features alone without the supporting contextual information provided by the BG. While large-scale pretraining improves robustness to some extent, recent work [56] shows that even Vision-Language Models (VLMs) like CLIP remain sensitive to BG distribution shifts. Figure 2 presents two examples: one where the context enables correct recognition, the other where misleading BG causes an incorrect prediction despite a clear FG object.² The nuanced role of BG is overlooked in recent object recognition literature [4, 4, 16, 16, 45, 45, 55, 55, 59, 59]. Commonly, frequent co-occurrences of FG and BG are dismissed as “spurious correlations”, a characterization we challenge as it ignores the important contribution of context to recognition.

We propose a novel approach to object recognition. It treats localization as an integral part of the recognition process, rather than something more challenging that should only follow classification. Our experiments show that zero-shot FG localization or even segmentation as part of recognition is often feasible with modern methods [19, 21, 26, 40, 41, 63], particularly in the context of fine-grained recognition. In the more general settings of datasets like ImageNet [12, 43] where images may contain many different objects, we demonstrate the potential of our approach by relying on GT prompts for object detection but without leaking the GT information into the classification model.

²CLIP-B predictions are from the online demo at https://huggingface.co/spaces/merve/compare_clip_siglip.

We first experimentally confirm that over-reliance on BG significantly hurts model robustness. We show that a straightforward approach – zero-shot BG removal – is a strong baseline. It outperforms or matches standard full image (FULL) modelling on a broad range of benchmarks. On the Spawrious [29] domain generalization benchmark it outperforms all state-of-the-art approaches that limit the influence of the BG by modifying their training procedure, often relying on additional BG annotations.

We proceed to show that by robustly incorporating BG information in form of the standard context-aware modelling into the FG-only recognition pipeline, the “Localize to Recognize Robustly” (L2R²) method can leverage the BG and further improve on in-distribution evaluation data, without loss of robustness to BG distribution shifts.

We further evaluate L2R² with non-parametric fusion on zero-shot object classification with multimodal VLMs. The method consistently improves the performance of diverse CLIP-like models on all datasets, including the recently introduced state-of-the-art SigLIP2 [52]. Notably, the performance of BioCLIP [48] on the extremely challenging FungiTastic [38] dataset doubles from 19 to 38 %.

The L2R² approach offers additional advantages. The decomposition opens new possibilities for BG modelling, such as leveraging large pretrained models with strong representations, like DINO [36] and CLIP [40], or incorporating diverse data sources, such as tabular metadata related to BG. This allows the BG component to capture context more effectively without extensive additional training, enhancing recognition in highly-varied environments.

The main contributions of this work are:

1. Introducing L2R², an object classification approach that models foreground (FG) independently of the context-aware FULL (which includes BG), enabling both robust and context-aware classification. FG and BG representations are combined through a simple, interpretable fusion module.
2. Demonstrating that zero-shot detection (without additional training data) can now be integrated into object recognition across a wide range of finegrained datasets.
3. Establishing FG as a strong baseline for BG suppression, improving performance of supervised classifiers across all benchmarks.
4. Showing that our approach improves on in-domain data while maintaining robustness to background shifts.
5. The same idea applied to zero-shot classification with large-scale VLMs significantly and consistently boosts the performance across multiple benchmarks.

2. Related work

Complementary role of FG and BG. Inspired by human vision, pioneering studies in object detection [13, 35, 51] emphasize the interdependence between FG and BG. These

works examine various types of contextual information and demonstrate how contextual cues provide critical insights for recognition, sometimes more so than the object itself. Acharya et al. [1] detect out-of-context objects through context provided by other objects within a scene, modelling co-occurrence through a Graph Neural Network (GNN).

In a recent study, Taesiri et al. [50] dissect a subset of the ImageNet dataset [43] into FG, BG, and FULL image variants using ground truth bounding boxes. A classifier is trained on each dataset variant, finding that the BG classifier successfully identifies nearly 75% of the images misclassified by the FG classifier. Additionally, they demonstrate that employing zooming as a test-time augmentation markedly improves recognition accuracy.

Closely related to our approach, Zhu et al. [64] advocate for independent modelling of FG and BG with post-training fusion. Unlike our method, which leverages recent advancements in zero-shot detection, their approach requires ground truth masks. A ground-truth-free approach is also proposed, but it consists of averaging 100 edge-based bounding box proposals for each classifier [65]. This is not only extremely costly but also benefits heavily from ensembling, not necessarily FG-BG decomposition. The experiments are limited to a subset of a single dataset and weaker baselines. In contrast, our work demonstrates the relevance and effectiveness of independent FG modelling fused with context-aware prediction in modern settings, even in the context of large-scale vision-language models.

Picek et al. [39] investigate the role of FG features and contextual metadata cues, such as time and location, in animal re-identification tasks. Unlike our general approach, their experiments specifically require the presence of ground-truth metadata, focus on niche applications and handcraft the BG models.

Asgari et al. [3] propose ‘MaskTune’, a method which promotes the learning of a diverse set of features by masking out discriminative features identified by pre-training, without explicitly categorizing these features as FG or BG.

Background suppression. Excessive reliance on BG has a detrimental impact on classifier robustness to distribution shifts [4, 7, 32, 45, 59]. In response, numerous strategies have been developed to mitigate this over-reliance by suppressing BG during classification. These methods typically involve regularizing classifier training to emphasize FG features, either through the use of ground-truth segmentations or attention maps [2, 7, 11, 61]. This enhances FG representation but prevents the classifier from learning BG cues that are necessary when FG is ambiguous. Moreover, when FG-BG correlations are strong, reliance on attention maps for segmentation proves problematic, as the attention often highlights the BG [33].

Another group of methods involves training classifiers on images with manipulated or out-of-distribution back-

grounds to reduce BG dependency [4, 16, 45, 55, 59]. This technique results in complete disregard of BG information or necessitates the modelling of FG-BG combinations for effective training, but it is not clear how to choose the optimal BG distribution.

Disentangling FG and context-aware modelling eliminates the need for BG suppression.

FG-BG in other tasks In the context of image segmentation, Mask2Former [8] also adopts the BG suppression approach implemented by masking out BG tokens in cross attention with queries inside the decoder to speed up convergence. The context is still incorporated in self-attention layers. A similar camouflage BG approach is adopted in [28]. More recently, Cutie [9] extends this masked attention approach by separating the semantics of the foreground object from the background for video object segmentation, focusing half of the object queries on the FG and half on the BG. While FG only masked attention improves over standard attention, the FG-BG masked attention outperforms both, showing the importance of BG information.

Unlike in image classification, the field of image segmentation and tracking combines BG suppression with contextual information, similarly to what we propose, but none adopts the independent FG and context-aware FULL modelling approach with robust fusion.

Reliance on BG in VLMs is analyzed by [56]. A dataset of animals, where each animal is associated with two kinds of BG, a ‘common’ one and a ‘rare’ one, where CLIP performance on the ‘rare’ BG drops significantly.

Zero-shot localization. Recent advancements in large vision-language models [26, 40] and class-agnostic, promptable image detection and segmentation [19, 21, 41, 63] now facilitate zero-shot object localization of a wide range of objects without knowing their (finegrained) class. This enables localization and effective FG-BG separation across a variety of image classification datasets.

Our methodology leverages these advances and seamlessly integrates robustness against unseen BGs and utilization of the contextual information in BG.

3. Method

We propose a novel approach to object recognition that decouples the modelling of the FG and the context-aware FULL representation of an image and then combines them in a lightweight interpretable module. Our approach consists of three stages, see Figure 3: 1. Image decomposition, 2. FG and FULL appearance modelling, and 3. Fusion.

3.1. Image decomposition

The goal of this stage is to localize the pixels representing the target object x_{FG} . The complement is the background context, x_{BG} . The decomposition relies on a zero-shot object detection model (referred to as f_D) such as

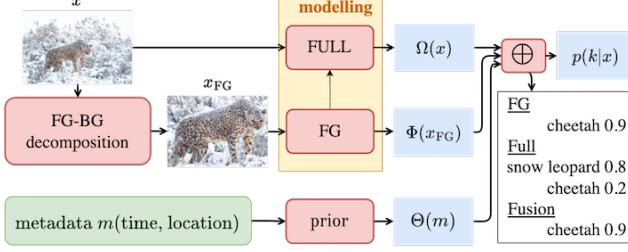


Figure 3. The “Localize to Recognize Robustly” approach to context-aware recognition – L2R² – proceeds in three stages: (1) decomposition of image x into FG and BG by zero-shot detection, possibly exploiting the predictions of FULL for prompt generation (2) independent modelling of the FG and the context-aware FULL (original image), which also serves as a fallback option when detection fails, and (3) fusion that robustly combines the representations from stage (2) to form the output prediction $p(k|x)$.

OWL [30, 31] or GroundingDINO [26]. These models are prompted by a dataset-specific text prompt p .

The operation of the image decomposition module can be described as

$$x_{FG}, x_{BG} = f_D(x, p) \quad (1)$$

Detector prompts. For each dataset, we generate an embedding created from either a single text meta-prompt, or an average of the embeddings of multiple ones. This works well in the case of fine-grained datasets where the objects belong to a specific meta-class (e.g., recognizing dog breeds or mushroom species). The detection in such cases is easy – a generic meta-prompt representing all classes (e.g., “dog” or “mushroom”) suffices. **Oracle prompts:** In experiments with general multi-object (and often also multi-label) datasets like ImageNet, we do not have a generally applicable solution. To show the potential of our decomposition approach, we pre-compute masks for all the datasets based on prompting each image with the text of its GT label.

Detailed settings for each dataset, together with a broader discussion and experiments with fully automated approaches, can be found in the Supplementary.

Fallback. L2R² relies on successful decomposition into FG and BG. Problematic detection can be flagged when the detector output is empty or the confidence falls below a threshold. In such cases, the output of L2R² is the standard FULL image prediction.

3.2. Subject and context-aware modelling

We opt for an approach where both the FG and FULL models Φ and Ω , respectively, output the per-class probability $p(k|x_{FG}) = \Phi(x_{FG})$ and $p(k|x_{FULL}) = \Omega(x_{FULL})$.

Another option explored in our experiments is the usage of a different modality representing the BG, in our case tabular metadata [5, 37].

Thanks to the decoupling of the FG and FULL modelling, the FG classifier can not learn BG shortcuts. It also increases interpretability - for instance, if we encounter an object from a well-known class in an unfamiliar environment and $p(k|x_{FULL})$ is expected to be low while the probability $p(k|x_{FG})$ is expected to be much higher.

3.3. Fusion modelling

The fusion model is designed to combine the outputs of base classifiers, typically FG and FULL, but we also experiment with BG (removing the FG pixels from FULL). The fusion model’s optimization is independent of the optimization of the fused models, simplifying the task. The fusion models are designed with interpretability in mind.

The fusion module can combine various models (e.g., FG+BG or FG+FULL). Let two pretrained models be denoted as Φ_1 and Φ_2 , which output logit vectors $\Phi_i(x) = z_i \in \mathbb{R}^C$. Applying softmax activations yields per-class confidences $\sigma(z_i)$. Predictions and their confidences are obtained by $\hat{y}_i = \operatorname{argmax}_{k \in \{1 \dots C\}} z_i^{(k)}$ and $\hat{p}_i = \sigma(z_i)^{(\hat{y}_i)}$.

Since deep neural networks are known to be poorly calibrated, potentially hindering model confidence comparisons, temperature-scaled logits [14, 17] are considered whenever applicable. Details and more fusion approaches are presented in Appendix B.3.

Higher confidence \oplus_{\max} : Selects the prediction with the highest confidence, setting $\hat{p} = \max(\hat{p}_1, \hat{p}_2)$.

Robust prediction \oplus_R : Selects \hat{y}_1 if $\hat{p}_1 > t$, otherwise $\max(\hat{p}_1, \hat{p}_2)$. The parameter t , where $t > 0$, can be optimized to maximize accuracy on the validation set or manually set to limit the influence of Φ_2 (typically BG).

Weighted logits \oplus_{WL} : Learns per-class weights $w_1, w_2 \in \mathbb{R}^C$, combining logits as $w_1 z_1 + w_2 z_2$. This approach trades off some of the interpretability for increased flexibility.

4. Implementation details

We provide two sets of experiments. The first one is conducted in the standard supervised training setup and the second one concerns large-scale pretrained VLMs in a zero-shot recognition setup. Additional details concerning the datasets and models are provided in the Appendix.

4.1. Datasets

We evaluate the L2R² recognition approach on 6 classification datasets, three of which are fine-grained:

FungiTastic (Fungi) [38]: A challenging fine-grained fungi species dataset with complex FG-BG relationships. The BG can be helpful in some cases but may be constant or less informative in others.

ImageNet-1K (IN-1K) [43]: A large dataset of diverse 1000 classes with diverse FG-BG relationships, many of them fine-grained. While IN-1K is the gold standard for

recognition model evaluation, it is known to contain many issues [22]. Therefore, we also evaluate on a ‘clean labels’ subset which only contains images where previous works correcting the dataset agree on the label [22].

Hard ImageNet (HIN) [33]: A subset of 15 IN-1K classes with strong FG-BG correlations. We also introduce two new test sets, Long Tail (HIN-LT) and Constant (HIN-CT), containing unusual or constant BGs.

CounterAnimal [56]: A dataset of 45 animal classes from IN-1K with images from the iNaturalist dataset. Each image is further labelled based on the BG as ‘common’ or ‘rare’.

Spawrious (Spaw) [29]: A synthetic dog-breed classification dataset introduced for domain generalization. Each class is associated with a specific BG type in the training set, but the BG distribution changes in the test set.

Stanford Dogs [20]: A dataset where the BG plays no obvious role in breed identification.

For datasets without a validation set (Dogs and Spaw), we reserve 10-15 % of the training set for validation. For ImageNet-1K, we adopt the official validation set as the test set, a common practice in the literature.

4.2. Supervised classification

Evaluation. Recognition accuracy is used as the main evaluation metric. For the highly imbalanced FungiTastic, macro-averaged accuracy (mean of per-class accuracies) is reported. The result is an average of five models with different seeds, except for ImageNet-1K where we use a single checkpoint from Timm.

Training - base classifiers. An independent classifier is learnt for FG and FULL (also BG for analysis). While this is not the most efficient approach – doubling the cost of training and inference – it gives us insights into how much can be learnt from different input kinds without being obfuscated by the impact of data augmentation, for example. A unified model with a shared backbone can be adopted in practice.

All models are based on the ConvNeXt V2-Base [27, 58] architecture from Timm [57], pretrained with a fully convolutional masked autoencoder (FCMAE) and fine-tuned on ImageNet-1k, unless indicated otherwise. The only exception is the ImageNet-1K dataset where we adopt the smaller ConvNeXt V2-Tiny variant for faster training. The input size is 224×224 and the batch size is 128 for all datasets.

We train models for each of the following inputs: FULL images, FG inputs (cropped bounding box padded to a square with a constant value to prevent distorting aspect ratios), and BG inputs (with FG shape obtained by prompting SAM [21] with the bounding box masked out). Each is trained with five different seeds and the results are averaged unless stated otherwise. Experiments with additional FG and BG representation are provided in the Appendix.

Fusion models. Fusion models combine base classifier outputs as per Section 3.3. The standard fusion combines FG



Figure 4. The unexpected role of shape in BG modelling. When investigating the results on the Hard ImageNet dataset, many examples were found where full image prediction is **incorrect** but *both* FG and BG (with shape) predictions are **correct**. Possible explanation: the mask provides the BG model with information about the location of the target object and its shape, information not available to unlike the full image model.

and BG (+FULL image classifiers as fallback option), though alternative combinations (e.g., FG + FULL) and different seed variations are also tested.

4.3. Vision-Language Models

We adopt the state-of-the-art SigLIP2 [52] (so400m-patch14-256 variant) for main experiments, with the exception of the FungiTastic dataset, where evaluating general-purpose models is not meaningful, their performance is very low regardless of the model. Instead, we adopt the BioCLIP [48] model for this dataset.

Unlike in the experiments with supervised models, no models are trained and there are no hyper-parameters; everything is zero-shot. We adopt the simplest ‘maximum confidence’ fusion \oplus_{\max} in all experiments.

FULL, FG and BG are processed by the same VLM and all results come from a model trained with the same seed since only one is publicly available. The input resolution to the models is 256×256 . FG inputs are padded to a square the same way as for supervised classifiers. Compared to standard classification, the model processes up to twice the number of images at inference.

Text prompts For each class c with a class name n_c , an embedding of the text ‘A photo of a n_c ’ is precomputed by the text encoder, which serves as the class prototype. Each image is then classified based on the nearest class prototype to the image embedding. We adopt the official class names provided by the dataset authors, no optimization of the class names was performed.

Evaluation. We report the macro-averaged accuracy (mean of per-class accuracies) for all datasets.

	HardImageNet*			Dogs	Spaw	ImageNet-1K*		Fungi	mean
	Original	Constant	Long-Tail	Original	Original	Original	Clean	Original	
FULL	97.33	90.51	81.33	90.28	43.20	82.35	92.01	43.17	77.52
FG	+0.46 97.79	-0.41 90.10	+4.60 85.93	+0.97 91.25	+48.11 91.31	+3.21 85.56	-0.02 91.99	-0.08 43.09	+7.11 84.63
BG	+0.51 97.84	-16.57 73.94	-1.60 79.73	-38.94 51.34	-40.58 2.62	-9.11 73.24	-10.73 81.28	-19.41 23.76	-17.05 60.47
FG \oplus *BG	+1.66 98.99	+1.61 92.12	+8.67 90.00	+0.99 91.27	+22.60 65.80	+4.78 87.13	+1.29 93.30	+2.48 45.65	+5.51 83.03
FG \oplus_{\max} BG	+1.44 98.77	+0.60 91.11	+8.67 90.00	-6.50 83.78	-17.30 25.90	+4.04 86.39	+1.01 93.02	-1.62 41.55	-1.21 76.31
FG \oplus_{WL} BG	+1.60 98.93	0.00 90.51	+9.11 90.44	-3.07 87.21	-15.49 27.71	+4.78 87.13	+1.29 93.30	+2.48 45.65	+0.09 77.61
FG \oplus_{R} BG	+0.78 98.11	+0.40 90.91	+5.66 86.99	+0.66 90.94	+48.05 91.25	+4.22 86.57	+1.17 93.18	-1.31 41.86	+7.45 84.98
FG \oplus *FULL	+1.52 98.85	-0.41 90.10	+7.43 88.76	+1.88 92.16	-0.20 43.00	+4.69 87.04	+1.75 93.76	+5.10 48.27	+2.72 80.24
FG \oplus_{\max} FULL	+1.39 98.72	-0.41 90.10	+7.79 89.12	+1.41 91.69	+33.46 76.66	+3.87 86.22	+1.49 93.50	+2.00 45.17	+6.38 83.90
FG \oplus_{WL} FULL	+1.68 99.01	+0.20 90.71	+8.05 89.38	+1.78 92.06	+33.75 76.95	+4.69 87.04	+1.75 93.76	+5.10 48.27	+7.12 84.65
FG \oplus_{R} FULL	+0.78 98.11	-0.61 89.90	+5.84 87.17	+1.38 91.66	+48.06 91.26	+4.03 86.38	+1.47 93.48	+1.56 44.73	+7.81 85.34

Table 1. Recognition accuracy of FG, BG, FULL and of several fusion models on Hard ImageNet, Stanford Dogs and Spawrious. For FungiTastic, which is highly imbalanced, the mean class accuracy is reported. The \oplus * fusion method is selected on the validation set. *Results with oracle detection obtained by GT prompting



Figure 5. Examples where FG model is **correct** and both full image and BG models are **incorrect** on Hard ImageNet - Long Tail.

ERM [53]	+6.14 77.49	JTT [25]	+18.89 90.24
GroupDRO [44]	+9.23 80.58	Mixup [60]	+17.13 88.48
IRM [C]	+4.10 75.45	Mixup [62]	+17.29 88.64
CORAL [49]	+18.31 89.66	L2R² (our)	
CausIRL [10]	+17.97 89.32	FULL	71.35
MMD-AAE [24]	+7.46 78.81	FG _C	+23.65 95.00
Fish [46]	+6.16 77.51	FG _M	+24.24 95.59
VREX [23]	+13.34 84.69	BG	-62.45 8.90
W2D [18]	+10.59 81.94	FG _C \oplus_{R} BG	+15.43 86.78

Table 2. Spawrious [29], a dataset with an adversarial BG shift – comparison to domain generalization methods. The **best** and **second best** results are highlighted. FG_C denotes cropping based on segmentation bbox, FG_M also removes the BG pixels from FG_C. All methods are initialized with the same ResNet50 model.

5. Results

5.1. Supervised training

An overview of both base and fusion models’ results on all test datasets is provided in Table 1.

Base models. The standard **FULL classification** provides a strong baseline across most datasets, with a moderate drop in performance on HIN-LT (-16%) and HIN-CT (-7%) compared to the original in-distribution test set. A more significant performance drop (from 99.9% to 43.2%) is observed on Spawrious between the validation and test set, where the model overfits to BG, which changes substantially between training and test sets. The **FG model** outperforms FULL by 7.11 % on average, either improving or maintaining performance around the FULL baseline on all datasets. As expected, the **BG model** generally performs worse than FULL and FG, but still very high due to the inclusion of the shape information. A notable exception is the Original HIN test set, where the BG is so correlated with the FG that the performance of BG matches FULL.

Images where BG works well while FG and FULL does not are presented in 4, images where only FG is correct are shown in 5.

Fusion models. The performance of different kinds of fusion is dataset-dependent, there is still a natural trade-off between in-domain gains and robustness to domain shift. Our findings can be summarized as: 1. The selection of the fusion method on the validation set provides close to optimal results with the exception of Spaw, where the training data does not contain any examples where the FG would be needed - there is no data to train the fusion models. 2. Even non-parametric \oplus_{\max} fusion works well on most datasets, but it can lead to significant performance drops on others, which hints at BG over-confidence. 3. Learnt fusion models like \oplus_{WL} lead to the strongest results, provided enough diverse training data. 4. For maximum robustness, \oplus_{R} is the best choice, as shown by its strong performance of Spaw, but the gains from context incorporation may be limited compared to the other methods. We also explored the im-

	HardImageNet			Dogs	Spaw	Fungi
	O	CT	LT	O	O	O
FULL	97.33	90.51	81.33	90.28	43.20	43.17
FG	97.79	90.10	85.93	91.25	91.31	43.09
FULL \oplus *FULL	97.51	90.91	82.89	91.13	40.00	48.54
FG \oplus *FG	97.91	89.9	86.58	91.9	94.62	47.24
FG \oplus *BG	98.99	92.12	90.0	91.27	65.81	45.65
FG \oplus *FULL	98.85	90.10	88.76	92.16	43.77	48.27

Table 3. Mean accuracy of L2R² models compared to different input models ensembles. O stands for the original test set.

pact of swapping the context-aware FULL model for the BG model in fusion. It sometimes works better, likely due to the explicit shape information or stronger learnt BG priors, but on most datasets, FULL leads to bigger performance gains and is more computationally efficient, as the BG model requires a segmenter.

Even though ‘oracle prompt’ detection was used for the ImageNet experiments, the results highlight how much progress on the dataset is blocked by a) localization capabilities of the classifier (and the images being multilabel) and b) lack of robust context handling. On the original validation set, FG improves over FULL by 3.21% and L2R² further improves over FG by 1.5%, reaching an accuracy of 87.04%. The performance of ConvNext V2-B from Timm, a model 3 \times larger than the Tiny variant presented here, is 84.9% on the original test set using the center crop data augmentation, which slightly inflates the performance.

Detailed results of the base classifiers (different FG, BG, and FULL image models), as well as additional fusion models, are presented in Appendix C.

Comparison to ensembling. A comparison of the L2R² FG \oplus *FULL approach to FULL \oplus *FULL and FG \oplus *FG is presented in Table 3.

Comparison to domain generalization methods. To provide a fair comparison of the L2R² approach for BG influence suppression to previous domain generalization methods, we provide results of Resnet50 classifiers and compare to the results from Spawrious [29] in Table 2. The FG (FG_C) model beats all the domain generalization methods by a large margin (4.8 %). Masking out the BG pixels based on a segmentation mask (FG_C) improves the performance further. The L2R² fusion FG \oplus R slightly reduces the performance compared to FG but it still outperforms FULL by 15% and leaves 7 out of the 12 domain generalization methods behind.

BG model with FungiTastic metadata This experiment explores an alternative approach to BG modelling based on tabular metadata. The FungiTastic dataset comes with such additional data, some of which are highly related to the BG appearance. Inspired by the metadata prior model of

[5, 37], we study the performance of incorporating various BG-related metadata, namely the habitat, substrate and month, with the FULL (as done by [5, 37]) and FG models. In summary, the method precomputes a prior probability of each class - metadata value combination and reweights the classifier predictions based on the metadata. The model assumes the appearance of the image is independent of the metadata, which is not true when the image BG is included (such as in the case of FULL). Combining with FG makes the method more principled.

Results in Table 4 show that all metadata kinds improve the performance of both models. The habitat helps the most, adding 3.8 % to the 43.5 % baseline of FULL and 4.2 % to the 44 % baseline of FG. For habitat and month, the improvements from metadata fusion are greater for the FG than for the FULL, even though the FG already performs better than FULL. We hypothesize this can be due to the suppression of BG influence in FG_C, leading to better FG-BG decoupling, as assumed by the metadata model.

	img	+habitat	+substrate	+month
FULL	43.50	47.26 +3.77	45.42 +1.92	45.19 +1.70
FG	44.00	48.22 +4.22	45.77 +1.77	45.80 +1.81

Table 4. Mean class accuracy of fusion models with BG representation [5, 37] based on tabular metadata (habitat, substrate, month) on the FungiTastic dataset. The increment over image-only performance is also reported. The results are averaged across 5 runs with different random seeds.

5.2. Zero-shot recognition with VLMs

An overview of zero-shot L2R² with BioCLIP (FungiTastic) and SigLIP2 (all other datasets) results is provided in Table 5. L2R² improves the performance of SigLIP2 on all datasets, except for the ‘rare’ test set of the CounterAnimal dataset. On average, the improvement is by 0.6% compared to FULL from 93.69 to 94.29%. The biggest gain is achieved on the Hard ImageNet - Long Tail test set, from 96.22 to 98.23% (2.01%).

The combination of FG with FULL overall outperforms FG with BG, possibly because the BG inputs may be out-of-distribution for the models, or because FULL also allows to benefit from ensembling different views of FG (FG + FULL can be viewed as (2 \times FG) + BG). On average there is no benefit from using FG only compared to FULL, the VLMs models are more robust to BG distribution shift than their supervised counterparts.

We also compare include the models performance with CenterCrop data augmentation. The results are comparable to FG on CounterAnimal, a dataset with a strong center bias, but performs much worse on the other datasets, confirming the necessity of explicit localization step.

	HardImageNet*			Dogs		Spaw		CounterAnimal		mean	Fungi	
	Original	Constant	Long-Tail	Original		Original		Common	Rare		Original	
SigLIP2-SO	←										BioCLIP	
FULL	95.33	100.00	96.22	84.11		95.34		95.50	89.36	93.69	18.62	
BG	-1.86 93.47	-10.54 89.46	-11.12 85.10	-62.37 21.74		-16.92 78.42		-11.49 84.01	-13.47 75.89	-18.25 75.44	-16.43 2.19	
FG	-2.53 92.80	+0.00 100.00	-1.67 94.55	+0.37 84.48		+1.33 96.67		-1.31 94.19	-0.92 88.44	-0.68 93.02	-1.75 16.87	
CENTERCROP	-4.00 91.33	-12.16 87.84	-7.03 89.19	-3.22 80.89		0.00 95.34		0.17 95.67	-1.20 88.16	-3.92 89.77	-0.19 18.43	
FG ⊕ _{max} BG	+1.34 96.67	+0.00 100.00	+1.57 97.79	+0.58 84.69		-0.41 94.93		-0.63 94.87	-2.61 86.75	-0.02 93.67	+14.92 33.54	
FG ⊕ _{max} FULL	+1.07 96.40	+0.00 100.00	+2.01 98.23	+0.97 85.08		+1.09 96.43		+0.17 95.67	-1.16 88.20	+0.59 94.29	+19.18 37.80	

Table 5. Mean accuracy (%) of maximum confidence fusion of FG + BG and FG + FULL on zero-shot classification with VLMs on different dataset test sets. Different kinds of inputs - FULL, FG and BG, are also reported. BioCLIP results are reported for fungi because general-purpose VLMs perform very poorly on such complex, niche datasets. *Results with oracle detection obtained by GT prompting.

Experiments with CLIP-B and CLIP-L can be found in Appendix C, as well as more insights on the somewhat counter-intuitive negative results on the CounterAnimal datasets, where one would expect BG removal to improve a lot on the ‘rare’ subset. Part of the problem can be attributed to some classes being hard to detect well, such as thin spiders, but there are also dataset construction issues as well which obfuscate the results.

5.3. Comparison to prior work

In all experiments, we aim to provide a fair comparison (such as the same training and inference procedure or the same amount of hyper-parameter tuning) between all models to show the benefits of the L2R² approach compared to an equivalent FULL object classification model. We abstain from claiming state-of-the-art on any of the datasets since we beat some previous methods simply through better hyper-parameter tuning. On others, such as the Stanford Dogs dataset, our models underperform because we reserve part of the training data for validation.

6. Conclusion

This paper introduced “Localize to Recognize Robustly”, L2R², an approach to object recognition where the benefits of context-aware recognition are combined with robustness to long-tail and out-of-domain BGs. L2R² incorporates zero-shot object localization into the recognition process, enabling the decoupling of FG and context-aware FULL modelling.

Our experiments demonstrate that zero-shot BG removal alone is a strong baseline for supervised models across diverse datasets, consistently outperforming standard full-image models in scenarios both with and without distribution shift. Notably, on the Spawrious [29] domain generalization benchmark, this approach surpassed all domain generalization baselines by a large margin – L2R² achieved an accuracy of 94.39%, while the runner-up achieved 90.24%.

Experiments with combined modelling further show that robustly incorporating BG information in form of context-aware FULL prediction to the aforementioned baseline further improves performance on all in-domain datasets with only a small trade-off in terms of robustness to BG distribution shift.

Finally, we show that the L2R² approach with parameter-free fusion applied to VLMs improves the performance of diverse CLIP-like models, including the state-of-the-art SigLIP2. Notably, the performance of the BioCLIP model on the FungiTastic dataset doubles, highlighting the potential of this approach in the biological domain.

Limitations. A primary limitation of this approach is its reliance on vision-language models in zero-shot object detectors, which may not generalize as well to very niche domains. We also discovered that current zero-shot object detectors do not allow us to apply the methodology to a fully general setup of datasets like ImageNet where images may contain many different objects.

We focused on demonstrating the benefits of the proposed approach, but the approach adopted in experiments with supervised learning introduces additional computational complexity by requiring two classifiers, which increases overhead compared to standard classification pipelines. Nonetheless our experiments with VLMs confirm the method works even when a single model is used for different kinds of inputs.

Future work. The research opens up the space for several directions of future work. First, we envision L2R² applied to more general settings in the context of object detection, either improving the detection classification head or building on top of class-agnostic detectors. Another area consists of exploring other possibilities of FG, BG and fusion modelling. For instance, occlusion can be removed in the FG space as part of the BG removal and occlusion data augmentation of the FG input consists of simply masking out portions of the image, without needing to model different textures. Efficiency improvements could leverage strong

pretrained representations, such as those in DINOv2 [36], to reduce computational demands. The increased computational cost can also be mitigated by only running the FULL classifier when FG is not confident.

References

- [1] Manoj Acharya, Anirban Roy, Kaushik Koneripalli, Susmit Jha, Christopher Kanan, and Ajay Divakaran. Detecting out-of-context objects using contextual cues. *arXiv preprint arXiv:2202.05930*, 2022. 1, 3
- [2] Ananthu Aniraj, Cassio F Dantas, Dino Ienco, and Diego Marcos. Masking strategies for background bias removal in computer vision models. In *Proceedings of the IEEE/CVF International Conference on Computer Vision*, pages 4397–4405, 2023. 1, 3
- [3] Saeid Asgari, Aliasghar Khani, Fereshte Khani, Ali Gholami, Linh Tran, Ali Mahdavi Amiri, and Ghassan Hamarneh. Masktune: Mitigating spurious correlations by forcing to explore. *Advances in Neural Information Processing Systems*, 35:23284–23296, 2022. 3
- [4] Andrei Barbu, David Mayo, Julian Alverio, William Luo, Christopher Wang, Dan Gutfreund, Josh Tenenbaum, and Boris Katz. Objectnet: A large-scale bias-controlled dataset for pushing the limits of object recognition models. *Advances in neural information processing systems*, 32, 2019. 1, 2, 3
- [5] Thomas Berg, Jiongxin Liu, Seung Woo Lee, Michelle L Alexander, David W Jacobs, and Peter N Belhumeur. Birdsnap: Large-scale fine-grained visual categorization of birds. In *Proceedings of the IEEE conference on computer vision and pattern recognition*, pages 2011–2018, 2014. 4, 7
- [6] Lucas Beyer, Olivier J Hénaff, Alexander Kolesnikov, Xiaohua Zhai, Aäron Van Den Oord, Google Brain, and Deepmind (London. Are we done with ImageNet? 2020. 13
- [7] Gaurav Bhatt, Deepayan Das, Leonid Sigal, and Vineeth N Balasubramanian. Mitigating the effect of incidental correlations on part-based learning. *Advances in Neural Information Processing Systems*, 36, 2024. 1, 3
- [8] Bowen Cheng, Ishan Misra, Alexander G Schwing, Alexander Kirillov, and Rohit Girdhar. Masked-attention mask transformer for universal image segmentation. In *Proceedings of the IEEE/CVF conference on computer vision and pattern recognition*, pages 1290–1299, 2022. 3
- [9] Ho Kei Cheng, Seoung Wug Oh, Brian Price, Joon-Young Lee, and Alexander Schwing. Putting the object back into video object segmentation. In *Proceedings of the IEEE/CVF Conference on Computer Vision and Pattern Recognition*, pages 3151–3161, 2024. 3
- [10] Mathieu Chevalley, Charlotte Bunne, Andreas Krause, and Stefan Bauer. Invariant causal mechanisms through distribution matching. *arXiv preprint arXiv:2206.11646*, 2022. 6
- [11] Po-Yung Chou, Yu-Yung Kao, and Cheng-Hung Lin. Fine-grained visual classification with high-temperature refinement and background suppression. *arXiv preprint arXiv:2303.06442*, 2023. 1, 3
- [12] Jia Deng, Wei Dong, Richard Socher, Li-Jia Li, Kai Li, and Li Fei-Fei. Imagenet: A large-scale hierarchical image database. In *2009 IEEE conference on computer vision and pattern recognition*, pages 248–255. Ieee, 2009. 2, 13
- [13] Santosh K Divvala, Derek Hoiem, James H Hays, Alexei A Efros, and Martial Hebert. An empirical study of context in object detection. In *2009 IEEE Conference on computer*

- vision and Pattern Recognition, pages 1271–1278. IEEE, 2009. 1, 2
- [14] Lior Frenkel and Jacob Goldberger. Network calibration by class-based temperature scaling. In *2021 29th European Signal Processing Conference (EUSIPCO)*, pages 1486–1490. IEEE, 2021. 4, 14
- [15] Robert Geirhos, Jörn-Henrik Jacobsen, Claudio Michaelis, Richard Zemel, Wieland Brendel, Matthias Bethge, and Felix A Wichmann. Shortcut learning in deep neural networks. *Nature Machine Intelligence*, 2(11):665–673, 2020. 1
- [16] Sreyan Ghosh, Chandra Kiran Reddy Evuru, Sonal Kumar, Utkarsh Tyagi, S Sakshi, Sanjoy Chowdhury, and Dinesh Manocha. Aspire: Language-guided data augmentation for improving robustness against spurious correlations. In *Findings of the Association for Computational Linguistics ACL 2024*, pages 386–406, 2024. 1, 2, 3
- [17] Chuan Guo, Geoff Pleiss, Yu Sun, and Kilian Q Weinberger. On calibration of modern neural networks. In *International conference on machine learning*, pages 1321–1330. PMLR, 2017. 4, 14
- [18] Zeyi Huang, Haohan Wang, Dong Huang, Yong Jae Lee, and Eric P Xing. The two dimensions of worst-case training and their integrated effect for out-of-domain generalization. In *Proceedings of the IEEE/CVF Conference on Computer Vision and Pattern Recognition*, pages 9631–9641, 2022. 6
- [19] Lei Ke, Mingqiao Ye, Martin Danelljan, Yu-Wing Tai, Chi-Keung Tang, Fisher Yu, et al. Segment anything in high quality. *Advances in Neural Information Processing Systems*, 36, 2024. 2, 3
- [20] Aditya Khosla, Nityananda Jayadevaprakash, Bangpeng Yao, and Li Fei-Fei. Novel dataset for fine-grained image categorization. In *First Workshop on Fine-Grained Visual Categorization, IEEE Conference on Computer Vision and Pattern Recognition*, Colorado Springs, CO, 2011. 5, 13
- [21] Alexander Kirillov, Eric Mintun, Nikhila Ravi, Hanzi Mao, Chloe Rolland, Laura Gustafson, Tete Xiao, Spencer Whitehead, Alexander C Berg, Wan-Yen Lo, et al. Segment anything. In *Proceedings of the IEEE/CVF International Conference on Computer Vision*, pages 4015–4026, 2023. 2, 3, 5, 14
- [22] Nikita Kisel, Illia Volkov, Katerina Hanzelkova, Klara Janouskova, and Jiri Matas. Flaws of imagenet, computer vision’s favourite dataset. *arXiv preprint arXiv:2412.00076*, 2024. 5, 13
- [23] David Krueger, Ethan Caballero, Joern-Henrik Jacobsen, Amy Zhang, Jonathan Binas, Dinghuai Zhang, Remi Le Priol, and Aaron Courville. Out-of-distribution generalization via risk extrapolation (rex). In *International conference on machine learning*, pages 5815–5826. PMLR, 2021. 6
- [24] Haoliang Li, Sinno Jialin Pan, Shiqi Wang, and Alex C Kot. Domain generalization with adversarial feature learning. In *Proceedings of the IEEE conference on computer vision and pattern recognition*, pages 5400–5409, 2018. 6
- [25] Evan Z Liu, Behzad Haghighi, Annie S Chen, Aditi Raghunathan, Pang Wei Koh, Shiori Sagawa, Percy Liang, and Chelsea Finn. Just train twice: Improving group robustness without training group information. In *International Conference on Machine Learning*, pages 6781–6792. PMLR, 2021. 6
- [26] Shilong Liu, Zhaoyang Zeng, Tianhe Ren, Feng Li, Hao Zhang, Jie Yang, Chunyuan Li, Jianwei Yang, Hang Su, Jun Zhu, et al. Grounding dino: Marrying dino with grounded pre-training for open-set object detection. *arXiv preprint arXiv:2303.05499*, 2023. 2, 3, 4, 14
- [27] Zhuang Liu, Hanzi Mao, Chao-Yuan Wu, Christoph Feichtenhofer, Trevor Darrell, and Saining Xie. A convnet for the 2020s. *Proceedings of the IEEE/CVF Conference on Computer Vision and Pattern Recognition (CVPR)*, 2022. 5
- [28] Naisong Luo, Yuwen Pan, Rui Sun, Tianzhu Zhang, Zhiwei Xiong, and Feng Wu. Camouflaged instance segmentation via explicit de-camouflaging. In *Proceedings of the IEEE/CVF conference on computer vision and pattern recognition*, pages 17918–17927, 2023. 3
- [29] Aengus Lynch, Gbètondji J-S Dovonon, Jean Kaddour, and Ricardo Silva. Spawrious: A benchmark for fine control of spurious correlation biases, 2023. 2, 5, 6, 7, 8, 13, 18
- [30] Matthias Minderer, Alexey Gritsenko, Austin Stone, Maxim Neumann, Dirk Weissenborn, Alexey Dosovitskiy, Aravindh Mahendran, Anurag Arnab, Mostafa Dehghani, Zhuoran Shen, et al. Simple open-vocabulary object detection. In *European Conference on Computer Vision*, pages 728–755. Springer, 2022. 4, 14
- [31] Matthias Minderer, Alexey Gritsenko, and Neil Houlsby. Scaling open-vocabulary object detection. *Advances in Neural Information Processing Systems*, 36, 2024. 4, 14
- [32] Mazda Moayeri, Phillip Pope, Yogesh Balaji, and Soheil Feizi. A comprehensive study of image classification model sensitivity to foregrounds, backgrounds, and visual attributes. In *Proceedings of the IEEE/CVF Conference on Computer Vision and Pattern Recognition*, pages 19087–19097, 2022. 3
- [33] Mazda Moayeri, Sahil Singla, and Soheil Feizi. Hard imagenet: Segmentations for objects with strong spurious cues. *Advances in Neural Information Processing Systems*, 35: 10068–10077, 2022. 3, 5, 13, 19
- [34] Mahdi Pakdaman Naeini, Gregory Cooper, and Milos Hauskrecht. Obtaining well calibrated probabilities using bayesian binning. In *Proceedings of the AAAI conference on artificial intelligence*, 2015. 14
- [35] Aude Oliva and Antonio Torralba. The role of context in object recognition. *Trends in cognitive sciences*, 11(12):520–527, 2007. 1, 2
- [36] Maxime Oquab, Timothée Darcet, Théo Moutakanni, Huy Vo, Marc Szafraniec, Vasil Khalidov, Pierre Fernandez, Daniel Haziza, Francisco Massa, Alaaeldin El-Nouby, et al. Dinov2: Learning robust visual features without supervision. *arXiv preprint arXiv:2304.07193*, 2023. 2, 9
- [37] Lukáš Pícek, Milan Šulc, Jiří Matas, Thomas S. Jeppesen, Jacob Heilmann-Clausen, Thomas Læssøe, and Tobias Frøsløv. Danish fungi 2020 - not just another image recognition dataset. In *Proceedings of the IEEE/CVF Winter Conference on Applications of Computer Vision (WACV)*, pages 1525–1535, 2022. 4, 7

- [38] Lukas Pícek, Klara Janouskova, Milan Sulc, and Jiri Matas. Fungitastic: A multi-modal dataset and benchmark for image categorization. *arXiv preprint arXiv:2408.13632*, 2024. 2, 4, 13, 16
- [39] Lukas Pícek, Lukas Neumann, and Jiri Matas. Animal identification with independent foreground and background modeling. *arXiv preprint arXiv:2408.12930*, 2024. 1, 3
- [40] Alec Radford, Jong Wook Kim, Chris Hallacy, Aditya Ramesh, Gabriel Goh, Sandhini Agarwal, Girish Sastry, Amanda Askell, Pamela Mishkin, Jack Clark, et al. Learning transferable visual models from natural language supervision. In *International conference on machine learning*, pages 8748–8763. PMLR, 2021. 2, 3
- [41] Nikhila Ravi, Valentin Gabeur, Yuan-Ting Hu, Ronghang Hu, Chaitanya Ryali, Tengyu Ma, Haitham Khedr, Roman Rädle, Chloe Rolland, Laura Gustafson, et al. Sam 2: Segment anything in images and videos. *arXiv preprint arXiv:2408.00714*, 2024. 2, 3
- [42] Robin Rombach, Andreas Blattmann, Dominik Lorenz, Patrick Esser, and Björn Ommer. High-resolution image synthesis with latent diffusion models. In *Proceedings of the IEEE/CVF conference on computer vision and pattern recognition*, pages 10684–10695, 2022. 13
- [43] Olga Russakovsky, Jia Deng, Hao Su, Jonathan Krause, Sanjeev Satheesh, Sean Ma, Zhiheng Huang, Andrej Karpathy, Aditya Khosla, Michael Bernstein, et al. Imagenet large scale visual recognition challenge. *International journal of computer vision*, 115:211–252, 2015. 2, 3, 4, 13
- [44] Shiori Sagawa, Pang Wei Koh, Tatsunori B Hashimoto, and Percy Liang. Distributionally robust neural networks for group shifts: On the importance of regularization for worst-case generalization. *arXiv preprint arXiv:1911.08731*, 2019. 6
- [45] Rakshith Shetty, Bernt Schiele, and Mario Fritz. Not using the car to see the sidewalk—quantifying and controlling the effects of context in classification and segmentation. In *Proceedings of the IEEE/CVF Conference on Computer Vision and Pattern Recognition*, pages 8218–8226, 2019. 1, 2, 3
- [46] Yuge Shi, Jeffrey Seely, Philip HS Torr, N Siddharth, Awni Hannun, Nicolas Usunier, and Gabriel Synnaeve. Gradient matching for domain generalization. *arXiv preprint arXiv:2104.09937*, 2021. 6
- [47] Sahil Singla and Soheil Feizi. Salient imagenet: How to discover spurious features in deep learning? In *International Conference on Learning Representations*, 2022. 1, 13
- [48] Samuel Stevens, Jiaman Wu, Matthew J Thompson, Elizabeth G Campolongo, Chan Hee Song, David Edward Carlyn, Li Dong, Wasila M Dahdul, Charles Stewart, Tanya Berger-Wolf, et al. Bioclip: A vision foundation model for the tree of life. In *Proceedings of the IEEE/CVF conference on computer vision and pattern recognition*, pages 19412–19424, 2024. 2, 5
- [49] Baochen Sun and Kate Saenko. Deep coral: Correlation alignment for deep domain adaptation. In *Computer Vision—ECCV 2016 Workshops: Amsterdam, The Netherlands, October 8–10 and 15–16, 2016, Proceedings, Part III 14*, pages 443–450. Springer, 2016. 6
- [50] Mohammad Reza Taesiri, Giang Nguyen, Sarra Habchi, Cor-Paul Bezemer, and Anh Nguyen. Imagenet-hard: The hardest images remaining from a study of the power of zoom and spatial biases in image classification. *Advances in Neural Information Processing Systems*, 36, 2024. 1, 3
- [51] Antonio Torralba. Contextual priming for object detection. *International journal of computer vision*, 53:169–191, 2003. 1, 2
- [52] Michael Tschannen, Alexey Gritsenko, Xiao Wang, Muhammad Ferjad Naeem, Ibrahim Alabdulmohsin, Nikhil Parthasarathy, Talfan Evans, Lucas Beyer, Ye Xia, Basil Mustafa, et al. Siglip 2: Multilingual vision-language encoders with improved semantic understanding, localization, and dense features. *arXiv preprint arXiv:2502.14786*, 2025. 2, 5
- [53] Vladimir Vapnik. Principles of risk minimization for learning theory. *Advances in neural information processing systems*, 4, 1991. 6
- [54] Vijay Vasudevan, Benjamin Caine, Raphael Gontijo-Lopes, Sara Fridovich-Keil, and Rebecca Roelofs. When does dough become a bagel? Analyzing the remaining mistakes on ImageNet. 13
- [55] Ke Wang, Harshitha Machiraju, Oh-Hyeon Choung, Michael Herzog, and Pascal Frossard. Clad: A contrastive learning based approach for background debiasing. *arXiv preprint arXiv:2210.02748*, 2022. 1, 2, 3
- [56] Qizhou Wang, Yong Lin, Yongqiang Chen, Ludwig Schmidt, Bo Han, and Tong Zhang. A sober look at the robustness of clips to spurious features. *Advances in Neural Information Processing Systems*, 37:122484–122523, 2025. 2, 3, 5, 13
- [57] Ross Wightman. Pytorch image models. <https://github.com/rwightman/pytorch-image-models>, 2019. 5
- [58] Sanghyun Woo, Shoubhik Debnath, Ronghang Hu, Xinlei Chen, Zhuang Liu, In So Kweon, and Saining Xie. Convnext v2: Co-designing and scaling convnets with masked autoencoders. In *Proceedings of the IEEE/CVF Conference on Computer Vision and Pattern Recognition*, pages 16133–16142, 2023. 5
- [59] Kai Xiao, Logan Engstrom, Andrew Ilyas, and Aleksander Madry. Noise or signal: The role of image backgrounds in object recognition. *arXiv preprint arXiv:2006.09994*, 2020. 1, 2, 3
- [60] Minghao Xu, Jian Zhang, Bingbing Ni, Teng Li, Chengjie Wang, Qi Tian, and Wenjun Zhang. Adversarial domain adaptation with domain mixup. In *Proceedings of the AAAI conference on artificial intelligence*, pages 6502–6509, 2020. 6
- [61] Shengying Yang, Xinqi Yang, Jianfeng Wu, and Boyang Feng. Significant feature suppression and cross-feature fusion networks for fine-grained visual classification. *Scientific Reports*, 14(1):24051, 2024. 1, 3
- [62] Huaxiu Yao, Yu Wang, Sai Li, Linjun Zhang, Weixin Liang, James Zou, and Chelsea Finn. Improving out-of-distribution robustness via selective augmentation. In *International Conference on Machine Learning*, pages 25407–25437. PMLR, 2022. 6

- [63] Xu Zhao, Wenchao Ding, Yongqi An, Yinglong Du, Tao Yu, Min Li, Ming Tang, and Jinqiao Wang. Fast segment anything. *arXiv preprint arXiv:2306.12156*, 2023. [2](#), [3](#)
- [64] Zhuotun Zhu, Lingxi Xie, and Alan L Yuille. Object recognition with and without objects. *arXiv preprint arXiv:1611.06596*, 2016. [1](#), [3](#)
- [65] C Lawrence Zitnick and Piotr Dollár. Edge boxes: Locating object proposals from edges. In *Computer Vision—ECCV 2014: 13th European Conference, Zurich, Switzerland, September 6–12, 2014, Proceedings, Part V 13*, pages 391–405. Springer, 2014. [1](#), [3](#)

A. Datasets

ImageNet-1K (IN-1K) [43]: A large dataset of diverse 1000 classes, many of which are fine-grained, such as over 100 species of dogs. The dataset features diverse FG-BG relationships. The ImageNet-1K has been tracking the progress of object recognition for more than 10 years. Alongside its wide adoption, it is known to contain many issues [6, 22, 54]. Recently, a unification of available error corrections was published [22]. Based on these unified labels, alongside the original dataset, we also evaluate on a ‘clean labels’ subset which only contains images where previous works correcting the dataset agree on the label.

Hard ImageNet (HIN) The Hard ImageNet dataset [33] is a subset of 15 ImageNet-1K classes [12] with strong FG-BG correlations, as observed in Single et al. [47]. GT segmentation masks are collected using Amazon Mechanical Turk. The objects in this dataset are less centered and the area they cover is below average. Of the ≈ 19000 training images we reserve 10% from each class for validation. The test set consists of 750 images.

For the purpose of assessing model robustness, we introduce two new test sets for this data set.

Hard ImageNet - Long Tail (LT) contains 226 images with unusual FG-BG combinations, such as “volleyball on snow”.

Hard ImageNet - Constant (CT) contains 99 images of essentially constant BGs (commonly co-occurring objects may still appear in the BG, such as snorkel and snorkel mask). See Figure 6 for example images.

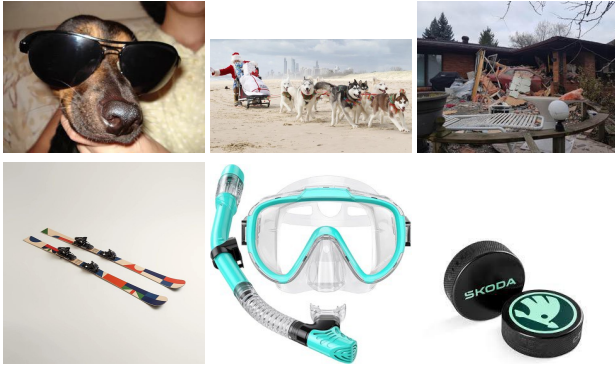


Figure 6. Images from the two new test sets for Hard ImageNet - Long Tail (top) and Constant background (bottom).

FungiTastic FungiTastic [38] is a challenging fine-grained unbalanced fungi species dataset with complex FG-BG relationships and naturally shifting distribution. In this paper we use the FungiTastic-Mini version of the dataset, where the train set contains observations collected until the end of 2021 (46842 images, 215 species), while the validation and test sets consist of observations from 2022 (9450

images, 196 species) and 2023 (10914 images, 193 species), respectively. For rare species, only few samples were collected in the training set, and may be missing in either validation or test set.

The dataset images are accompanied by diverse metadata such as time, GPS location, habitat, substrate, EXIF or toxicity level. The time, substrate and habitat attributes are used to estimate the class priors in some of our experiments.

Spawrious The Spawrious datasets [29] consist of images with strong FG-BG correlations generated using *Stable Diffusion v1.4* [42]. We demonstrate our method on the O2O-E Env1 dataset, where each of the 4 dog breed classes is associated with one of the 4 different backgrounds (*Desert, Jungle, Dirt, Snow*) in the training set.

The BGs are permuted in the test set, creating a significant domain shift.

Two variations of the Spawrious dataset are analyzed:

- For the Resnet-50 experiments in Tables 15 and 2 we follow the process of [29] in which training set FG-BG combinations are set to 97% (e.g. *Bulldogs* appear in *Desert* 97% of the time, and on *Beach* 3% of the time), while test set images for one class always contain the same BG (test *Bulldogs* always appear on *Dirt* BG). See [29][Table 2] for more details.
- For the rest of our Spawrious experiments, including Tables 1 and 14, the training correlations are set to 100% as well.

Of the 12672 images in the initial training set, 10% are reserved for validation.

Stanford Dogs The Stanford Dogs dataset [20], a curated subset of [12], contains 20, 580 images of dogs from around the world belonging to 120 species, with $\approx 150 - 200$ images per class. A large portion of settings are in man-made environments, resulting in larger BG variation compared to other animal datasets. There are no strong FG-BG correlations that we are aware of.

Counter Animal A dataset of 45 animal classes from IN-1K with images from the iNaturalist collection of wildlife images introduced in [56]. Each image is further labelled based on the BG as ‘common’ or ‘rare’. To construct the dataset, the researchers first checked CLIP’s accuracy on the images and then identified which types of backgrounds are present in images with low accuracy. The construction process disregards the fact that there can be many reasons for the accuracy drop and that BG changes are often highly correlated with a change in appearance - for instance, photos of birds in the sky are typically captured mid-flight, from greater distance than on the ground, and in a very different pose. Often, the animals in the ‘rare’ group are captured in an environment where they are hard to localize even for humans due to camouflage, while the common subset captures them on a white background. Overall, for many classes, it is not clear whether it is the change in BG distribution or the

change in FG distribution that causes the accuracy drop.

We illustrate some of the issues on randomly sampled images in Figure 7. The dataset also contains many duplicate images or images where the animal is not even visible.

B. Methods

B.1. Localization

Fine-grained datasets and Counter Animal The detections are produced by the open-set object detector Grounding DINO [26] from dataset-specific text prompts, as discussed in the main text. For Stanford Dogs and Spawrious datasets, segmentation masks are generated with the text prompt ‘full dog’ while the prompt ‘mushroom’ is used for the FungiTastic.

For Counter Animal, the prompt is composed as an average of the embeddings of the following meta-prompts: ‘animal’, ‘bird’, ‘insect’, ‘reptile’.

Hard ImageNet GroundingDINO works well in cases when it is known a priori that an object matching the text exists in the image. Otherwise, it is prone to output false positives. This is the case for Hard ImageNet, where we prompt an image with texts corresponding to multiple labels. Then, false positive FG outputs (e.g. a person) correlated to a different class (e.g. sunglasses) may confuse the model. To mitigate this, we replace Grounding DINO with the OWLv2 detector [30, 31], at the expense of introducing more false negatives. A comparison of OWLv2 and GroundingDINO in terms of average number of object proposals per image is provided in Figure 11.

When a segmentation mask is required, such as for experiments that consider BG with shape inputs, we prompt the SAM [21] model with the detected bounding boxes.

B.2. Input options

We extend the different methods to create the x , x_{FG} , x_{BG} images introduced in the main text. These are input options for the FULL, FG and BG base classifiers, and represent the rows in Tables 9-12. The different options are:

1. FULL images - the standard approach.
2. FG_C : the image is cropped according to the bounding box and padded to a square to preserve the aspect ratio.
3. FG_M : the BG is fully masked before cropping a square bounding box.
4. BG_S : BG images with shape (the FG are masked, but their shapes remain)
5. BG_B : BG w/o shape (a minimal segmentation bounding box masks the FG)

A visualization is presented in Figure 9.

B.3. Combined models

Here we present the fusion models in detail, including the temperature-scaled variants.

We consider two fixed trained models: Φ_1 and Φ_2 , which output logit vectors $\Phi_i(x) = z_i \in \mathbb{R}^C$, to which softmax activations are applied: $\sigma(z_i)$. Predictions are obtained by $\hat{y}_i = \operatorname{argmax}_k z_i^{(k)}$ and their confidences by $\hat{p}_i = \max_k \sigma(z_i)^{(k)}$, $i = 1, 2$.

Since the predictions may be over/under-confident (i.e. the confidences do not reflect the accuracies) and we want to compare the confidences of different models, we opt for calibrating them using the method of *temperature scaling* [17]. This is done using a single parameter $T > 0$ for all classes. Given a model Φ , the logits and confidences are scaled by

$$z \rightarrow z/T, \sigma(z) \rightarrow \sigma(z/T), \hat{p} \rightarrow \tilde{p} = \max_k \sigma(z/T)^{(k)} \quad (2)$$

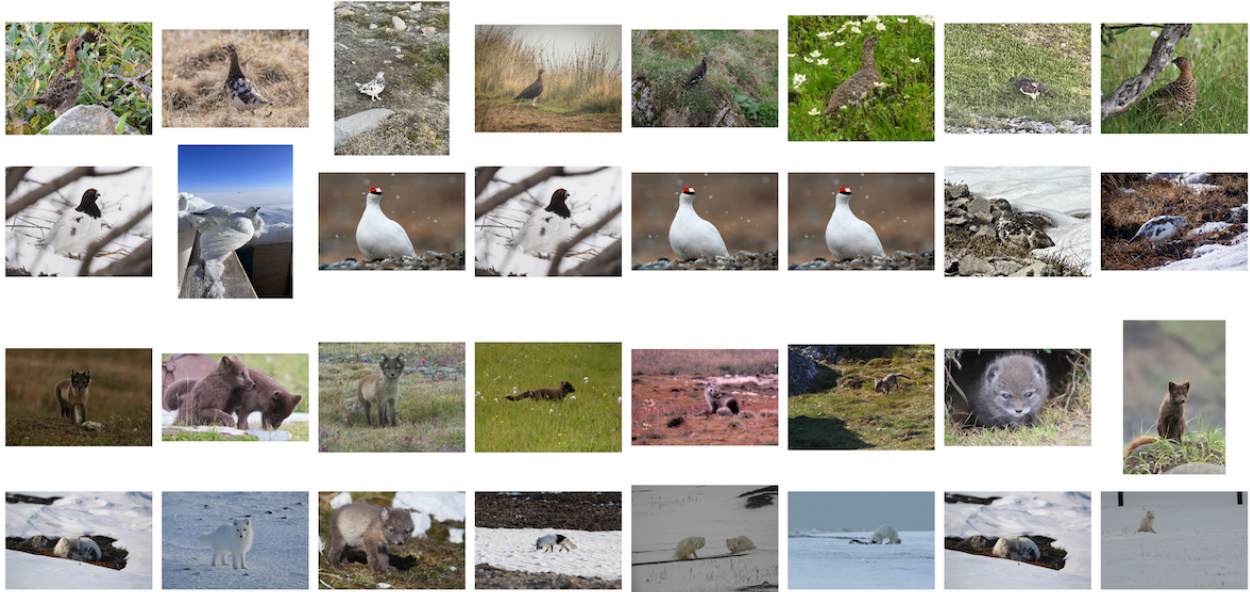
Note that the predictions of a fixed model do not change, since the same parameter is applied to all classes. This parameter T is optimized such that the cross entropy loss is minimized on the *validation* set.

For some datasets it may be desirable to apply different scaling parameters for each class. Such a *class-based temperature scaling* calibration methods was proposed in [14], attempting to minimize the *expected calibration error* (ECE) [34] on the validation set, while not decreasing accuracy, by performing a greedy grid-search. This results in modified logits:

$$z = (z^{(1)}, \dots, z^{(C)}) \rightarrow (z^{(1)}/T_1, \dots, z^{(C)}/T_C) \quad (3)$$

Confidence fusion

1. (Max confidence) Between \hat{y}_1 and \hat{y}_2 choose the most confident prediction \hat{y}_i , i.e. the one with confidence $\hat{p}_i = \max(\hat{p}_1, \hat{p}_2)$.
2. (Max scaled confidence) Again we choose the more confident prediction \hat{y}_i , but now the confidences are calibrated using temperature scaling from Equation (2), originating from $z_1/T_1, z_2/T_2$, i.e. choose the one with $\tilde{p}_i = \max(\tilde{p}_1, \tilde{p}_2)$.
3. (Threshold prediction) We choose \hat{y}_1 if $\hat{p}_1 > t$, otherwise choose the higher confidence prediction. Here $t > 0$ is a parameter maximizing the new prediction accuracy on the validation set.
4. (Temperature-scaled average) Let $z_1/T_1, z_2/T_2$ be the scaled logits vectors from Equation (2) from the two models and take the average $\frac{1}{2}(\sigma(z_1/T_1) + \sigma(z_2/T_2))$. The prediction is given by argmax as usual.
5. (Temperature-scaled weighted average) As before, but take a weighted average $\alpha\sigma(z_1/T_1) + (1 - \alpha)\sigma(z_2/T_2)$,



Animals like polar foxes change appearance between winter ('snow') and summer ('grass').



The pose of flying birds is very different from those on the ground.



Green iguanas on a green background, often hidden among leaves, are hard to spot even for a human.

Figure 7. Common problems in the counter animal dataset. Each row shows a random sample of images from a class/BG combination. The top row of images always shows images from the 'rare' BG group while the bottom row shows images from the same class, 'common' BG subset.

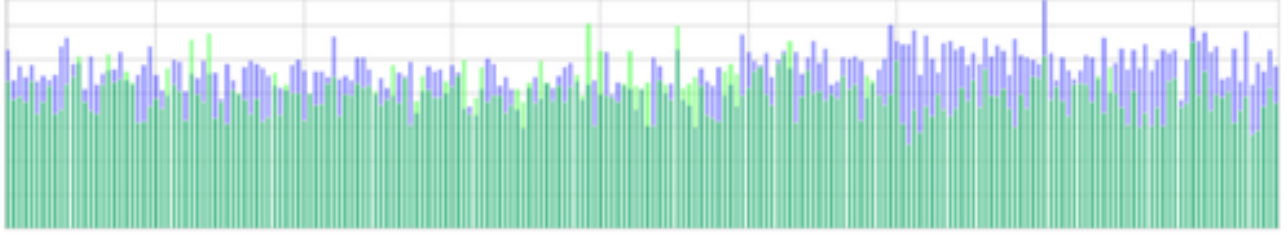


Figure 8. The relative role of **FG** and **BG** for the 215 FungiTastic classes shown by the weights of the learned weighted logits combination model, i.e. Model 9. in Section B.3. The BGs has a higher weight for about 15%



Figure 9. Different kinds of input to the FG and BG models. FULL is the standard full image, FG_C is cropped based on the segmentation bounding box, FG_M is same as FG_C but with the BG regions masked out, BG_S is the shape-preserving BG model with FG regions masked out and BG_B has the area corresponding to the the segmentation bounding box masked out.

where $\alpha \in [0, 1]$ maximizes validation set prediction accuracy.

Learnt fusion Finally, the predictions learned from the combined logits on the train set are:

8. (Concatenate + FC layers) To model the interaction between outputs of Φ_1 and Φ_2 , we create new (train, validation and test) datasets by concatenating the logits for each sample x :

$$\Psi(x) = (\Phi_1(x), \Phi_2(x)) = (z_1, z_2) = (z_1^{(1)}, \dots, z_1^{(C)}, z_2^{(1)}, \dots, z_2^{(C)}) \in \mathbb{R}^{2C} \quad (4)$$

We input Equation (4) into a shallow fully connected network, whose weights are learned from the training set, with cross entropy loss. This can learn more flexible combinations, but it lacks in interpretability and may overfit if the number of classes is large.

9. (Weighted logits combination) Generalizes the averages from confidence fusion by allowing the weights to be class-dependent vectors $w_1, w_2 \in \mathbb{R}^C$, representing combined logits as $w_1 z_1 + w_2 z_2 =$

$$(w_1^{(1)} z_1^{(1)} + w_2^{(1)} z_2^{(1)}, \dots, w_1^{(C)} z_1^{(C)} + w_2^{(C)} z_2^{(C)}).$$

We optimize the cross entropy loss instead of the ECE from Equation (3), so gradient descent becomes applicable replacing the grid search. We optimize the weights on the training set instead of the validation set. Compared to the FC model 8, there are much fewer param-



Figure 10. Extreme BG overfitting on the Fungitastic dataset [38]. Both the FULL (middle column, expected) and BG (right column, surprising) images are correctly classified, with high confidence. The likely reason is the presence of a unique “background” feature, the hand (bottom left) and the existence of a training image (taken in a different year) acquired from a very similar viewpoint (top left). The problem highlights the benefits of the interpretability of L2R²: with uncertain FG prediction, one should not pick and eat the mushroom no matter how confident the FULL or BG predictions are. Note: the mushrooms in each row are the same species.

eters, so there is less risk of overfitting and the network weights are more interpretable (see Fig. 8).

C. Additional experiments

C.1. Supervised learning

The setup of the experiments is described in the main text, where only a summary of the results was reported. Ex-

	HardImageNet*			Dogs	Spaw	CounterAnimal		Fungi
	Original	CT	LT	Test	Test	Common	Rare	Original
CLIP-B								
FG \oplus_{\max} BG	+2.4 88.93	-1.7 87.88	+6.82 84.51	+7.56 58.09	+4.05 89.86	+0.57 84.08	-0.29 67.75	+1.07 2.82
FG \oplus_{\max} FULL	+2.8 89.33	+2.34 91.92	+6.82 84.51	+7.0 57.53	+4.74 90.55	+2.18 85.69	+0.54 68.58	+1.91 3.66
Bg	-5.2 81.33	-33.71 55.87	-21.38 56.31	-45.43 5.10	-46.83 38.98	-13.35 70.16	-15.08 52.96	-0.74 1.01
FG	-0.53 86.00	-2.46 87.12	+1.69 79.38	+7.5 58.03	+5.26 91.07	-1.92 81.59	+0.32 68.36	+0.05 1.80
FULL	86.53	89.58	77.69	50.53	85.81	83.51	68.04	1.75
BioCLIP								
FG \oplus_{\max} BG	-0.4 19.60	-2.61 14.14	-1.39 15.93	-0.39 2.84	+0.10 40.83	-0.16 82.29	-2.73 75.63	+14.92 33.54
FG \oplus_{\max} FULL	+0.27 20.27	+2.44 19.19	-2.72 14.60	-0.18 3.05	+0.91 41.64	+2.27 84.72	-0.08 78.28	+19.18 37.80
BG	-1.73 18.27	-9.10 7.65	-6.99 10.33	-2.30 0.93	-3.03 37.70	-21.25 61.20	-20.21 58.15	-16.43 2.19
FG	-5.87 14.13	+0.89 17.64	-3.69 13.63	+0.03 3.26	+0.92 41.65	-3.90 78.55	-4.08 74.28	-1.75 16.87
FULL	20.00	16.75	17.32	3.23	40.73	82.45	78.36	18.62
CLIP-L								
FG \oplus_{\max} BG	+1.34 94.27	+1.41 94.95	+3.52 93.36	+5.10 73.25	+0.15 94.89	-0.33 92.64	+0.85 85.17	+1.42 3.10
FG \oplus_{\max} FULL	+2.40 95.33	+1.41 94.95	+3.97 93.81	+4.62 72.77	+0.69 95.43	+0.38 93.35	+1.12 85.44	+2.26 3.94
BG	-2.53 90.40	-29.51 64.03	-16.52 73.32	-59.15 9.00	-24.14 70.60	-15.74 77.23	-16.55 67.77	-1.20 0.48
FG	-0.66 92.27	+1.02 94.56	-1.76 88.08	+5.08 73.23	+0.71 95.45	-0.99 91.98	+0.23 84.55	+0.11 1.79
FULL	92.93	93.54	89.84	68.15	94.74	92.97	84.32	1.68
SigLIP2-SO								
FG \oplus_{\max} BG	+1.34 96.67	+0.00 100.00	+1.57 97.79	+0.58 84.69	-0.41 94.93	-0.63 94.87	-2.61 86.75	—
FG \oplus_{\max} FULL	+1.07 96.40	+0.00 100.00	+2.01 98.23	+0.97 85.08	+1.09 96.43	+0.17 95.67	-1.16 88.20	—
BG	-1.86 93.47	-10.54 89.46	-11.12 85.10	-62.37 21.74	-16.92 78.42	-11.49 84.01	-13.47 75.89	—
FG	-2.53 92.80	+0.00 100.00	-1.67 94.55	+0.37 84.48	+1.33 96.67	-1.31 94.19	-0.92 88.44	—
FULL	95.33	100.00	96.22	84.11	95.34	95.50	89.36	—

Table 6. Performance of VLM models on different kinds of inputs - FULL, FG and BG. Maximum confidence fusion of FG + BG, as well as FG + FULL, is also reported. — SigLIP2 results were left out due to the high GPU memory requirements on datasets with a high number of classes. *Results obtained with oracle detections generated by GT prompting.

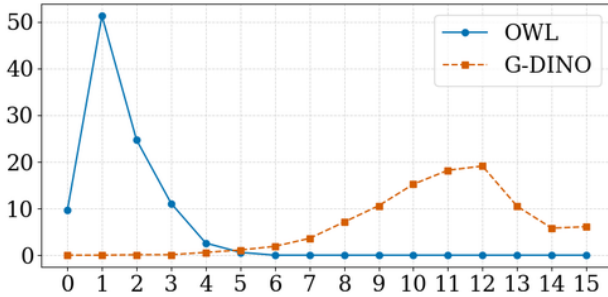


Figure 11. Object detection by OWL+SAM and GroundingDino+SAM on the Hard ImageNet validation set (≈ 1900 images). For each image, the zero-shot detector is prompted for each class, producing $s \in (0, \dots, 15)$ non-empty segmentation masks. The histogram of the s values is shown. For example, 51.3% of images get a single OWL+SAM mask. The GroundingDINO results show a higher number of masks. The value of k is optimized on the validation set.

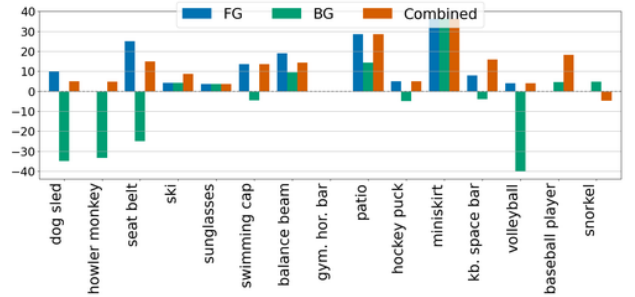


Figure 12. Per-class accuracy % increase or decrease w.r.t. full-image performance on the proposed HardImageNet test set with a significant BG distribution shift. The experiment confirms that FG_C (cropping image based on segmentation bounding box) is a strong baseline, adding 5.5% in accuracy. The combined approach performs the best, adding 8 % of accuracy. Surprisingly, the BG classifier performs well on about half of the classes, probably due to the information preserved by the mask shape, despite the domain shift.

haustive results of all the base and fusion classifiers for all datasets are reported in Tables 9 - 14.

Stanford Dogs. Our experiments show that the context (BG without shape) plays little role in breed identification on this

HardImageNet Test Sets				
Model		Original	Long Tail	Constant
FULL		97.33	81.33	90.51
GT masks	FG	97.63	87.08	94.55
	BG	95.01	78.94	67.88
	FG \oplus BG	98.45	89.56	90.30
GT labels	FG	97.79	85.93	90.10
	BG	97.84	79.73	73.94
	FG \oplus BG	98.99	90.0	92.12
No GT	FG	95.55	81.24	90.1
	BG	96.83	80.27	88.28
	FULL \oplus FG	97.68	90.91	83.45
	FULL \oplus FG \oplus BG	98.03	83.63	91.31
	FULL \oplus *FULL	97.51	90.91	82.89

Table 7. Accuracy on the HardImageNet dataset with different segmentation setups. (top) GT masks, (middle) prompting with GT labels, (bottom) prompting with top- k predictions of full image classifier without any ground truth labels or mask.

dataset, see Table 12.

Resnet50 experiments on Spawrious. These additional experiments use a LR of 10^{-5} . As explained in Subsection A, we set the training set FG-BG correlations to 97% to compare with the results in [29][Table 2]. The Resnet50 models are initialized with two sets of pretrained weights: from Timm and from torchvision. The results are recorded in Table 15³.

Hard Imagenet with GT masks. This setting provides an upper bound for the “detection during recognition” approach. The results are collected in Table 11. The original test set has strong FG-BG correlations, and therefore BG classifiers score very high by themselves and FG+BG performs best. On the long-tailed BGs test set, BG underperforms, but the FG + BG fusion still dominates. On the CT BG test set all fusion models unsurprisingly underperform the FGs.

Hard Imagenet without GT prompt mask generation

We also provide results of experiments with automatic FG-BG generation in the general setup of object recognition on images with many different objects on the Hard ImageNet dataset.

Mask generation: The FULL classifier’s top- k predictions guide the segmentation prompt generation. Let C be the number of classes. Each class $i \in \overline{1, C}$ is described by a

³The results in Table 15 are not directly comparable with Table 14 because FG-BG correlations are set differently. Also, the results slightly differ from those in the main text, where a sub-optimal learning rate for the FULL model was used. This does not affect any of the conclusions

	Test	Test LT	Test CT
FG OWL	95.55%	81.24%	90.10%
FG G-DINO	94.27%	78.32%	88.89%
BG OWL	96.83%	80.27%	88.28%
BG G-DINO	95.20%	69.47%	83.84%
Fusion OWL	98.03%	83.63%	91.31%
Fusion G-DINO	97.87%	80.09%	90.91%

Table 8. HardImageNet with automatic FG-BG generation and comparison of OWL vs GroundingDino for object proposal generation. Fusion consists of FULL+FG+BG.

text prompt p_i . For each sample, we consider the top- k predictions $\{i_j\}_{j=1}^k$ of the FULL model based on the confidence scores. These are the candidate labels for the final prediction and we prompt the detector with each of them, resulting in a FG and BG for each candidate. When the detector output is empty, FG and BG are replaced by the full image.

Fusion: Unlike in the GT prompting/GT masks setup, the fusion now needs to take multiple candidates into account.

We tried applying the same fusion methods as in the main paper to each candidate individually, selecting the one with the highest fusion confidence as the output, but this approach does not outperform the FULL baseline. This is likely caused by poor calibration of the fusion model output.

We provide an alternative hand-crafted fusion strategy which leads to positive results, but we do not claim it as a contribution and it may not transfer to other datasets:

Given an image x we aggregate logits for FG and BG predictions as follows. Using the top- k prompts $\{p_{i_j}\}_{j=1}^k$ we generate $x_{FG_{i_1}}, \dots, x_{FG_{i_k}}$ by equation (1),⁴ which provide a list of output logits $\Phi(x_{FG_{i_1}}), \dots, \Phi(x_{FG_{i_k}}) \in \mathbb{R}^C$ using the FG-trained model Φ . From each of these vectors we record only the entry of the class of the prompt which generated it, i.e. entry i_j from $\Phi(x_{FG_{i_j}})$. Selecting these, and following the same process for the BG model Ψ we obtain aggregated logits

$$\begin{aligned} z_{FG} &:= \left(\Phi(x_{FG_{i_1}})^{(i_1)}, \dots, \Phi(x_{FG_{i_k}})^{(i_k)} \right) \\ z_{BG} &:= \left(\Psi(x_{BG_{i_1}})^{(i_1)}, \dots, \Psi(x_{BG_{i_k}})^{(i_k)} \right) \end{aligned} \quad (5)$$

The FG and BG predictions are i_ℓ where $\ell = \arg\max_j z_{FG}^{(j)}$, respectively $\ell = \arg\max_j z_{BG}^{(j)}$.

For the fusions we combine (5) with the original full image top- k logits $z_{Full} := (z_{i_1}, \dots, z_{i_k})$ by averaging $3z_{Avg} := z_{Full} + z_{FG} + z_{BG}$ or $2z_{Avg} := z_{Full} + z_{FG}$. The leads to prediction i_ℓ if $\ell = \arg\max_j z_{Avg}^{(j)}$.

⁴If an image and prompt p_i fail to generate x_{FG_i}, x_{BG_i} using the detector then they default (fallback) to $x_{FG_i}, x_{BG_i} := x$.

The results are provided in Table 7. An OWL vs Grounding DINO detector comparison is provided in Table 8, showing the superiority of OWL in this setup.

FungiTastic. Since this dataset is highly unbalanced, we report the macro-averaged accuracy as the main metric. Due to some rare species, the number of present classes is smaller on the validation and test sets. The *torchmetrics* implementation of the metrics, which we rely on in other experiments, does not account for such a scenario and the metric is implemented manually. Missing classes are removed before averaging the per-class accuracies on the validation and test sets.

The results are summarized in Table 9. The highest mean accuracy is attained by the FG + FULL combination. This shows that the BG information (which is part of FULL) is important for this dataset as well.

The learnt weights of the weighted logits fusion model on the FungiTastic dataset are visualized in Figure 8.

Segmentation ablation on Hard Imagent. In Table 7, a comparison of the fully-automated segmentation to cheating segmentation setups is provided. In the first set of experiments, ground truth segmentation masks from [33] are used to both train and evaluate all the models. In the second set of experiments, ground truth labels are used to create segmentation prompts during both training and evaluation. The last set of experiments is the standard fully-automatic setup which does not use any ground truth.

Surprisingly, the cheating setup with labels sometimes outperforms the ground truth masks. We hypothesize this can be attributed to the poor quality of the GT masks (coarse), compared to the outputs of SAM (clear shape).

Per-class analysis on Hard ImageNet where FG, BG and fusion model performance is compared to FULL on new test sets with strong BG shift using GT masks is provided in Figure 12. Examples of **extreme overfitting to BG on FungiTastic** are shown in Figure 10.

C.2. Vision-Language Models

A comparison of CLIP-B (openai/clip-vit-base-patch32), BioCLIP (imageomics/bioclclip), CLIP-L (openai/clip-vit-large-patch14) and SigLIP2-SO (timm/ViT-SO400M-16-SigLIP2-256) are presented in Table 6. The results show that L2R² with FG \oplus_{\max} FULL fusion consistently improves performance across all test sets. The only exceptions are the ‘rare’ CounterAnimal test set for some of the models and BioCLIP, which was trained for very different domains than most of the datasets. On its target domain, the FungiTastic, its performance doubles with L2R². The biggest gains are achieved for the smallest CLIP-B model, whose performance is significantly lower on average.

Dataset	Val acc	Val avg acc	Test acc	Test avg acc
FULL	68.31% \pm 0.62	45.42% \pm 0.61	66.82% \pm 0.82	43.17% \pm 1.24
FG _C	68.33% \pm 0.59	45.56% \pm 0.69	66.58% \pm 0.47	43.09% \pm 0.39
FG _M	64.99% \pm 0.39	42.14% \pm 0.48	63.45% \pm 0.55	39.02% \pm 0.8
BG _S	45.26% \pm 2.92	24.73% \pm 2.42	43.1% \pm 2.42	23.76% \pm 2.07
BG _B	21.79% \pm 0.34	10.94% \pm 0.38	19.84% \pm 0.3	10.77% \pm 0.47
FG _C \oplus BG _S				
Max conf	68.08% \pm 0.22	43.54% \pm 1.5	66.23% \pm 0.26	41.55% \pm 1.02
Max scaled conf	68.0% \pm 0.46	43.37% \pm 0.9	66.06% \pm 0.27	41.26% \pm 0.52
Threshold conf	68.24% \pm 0.47	44.09% \pm 0.92	66.35% \pm 0.33	41.86% \pm 0.45
TempScaled AvgPred	68.92% \pm 0.45	44.24% \pm 0.85	66.92% \pm 0.24	41.9% \pm 0.48
TempScaled WeightedAvg	69.52% \pm 0.46	45.43% \pm 0.59	67.55% \pm 0.24	43.17% \pm 0.46
Concatenate + FC layers	68.87% \pm 0.25	47.56% \pm 0.57	67.15% \pm 0.41	43.31% \pm 1.0
WeightedLogitsComb	70.47% \pm 0.17	48.65% \pm 0.52	68.58% \pm 0.39	45.65% \pm 0.35
Best - WeightedLogitsComb		48.65% \pm 0.52		45.65% \pm 0.35
Oracle	74.19% \pm 0.49	50.77% \pm 0.69	72.46% \pm 0.41	48.88% \pm 0.94
FG _C \oplus FULL				
Max conf	71.47% \pm 0.43	47.34% \pm 1.04	69.64% \pm 0.35	45.17% \pm 0.88
Max scaled conf	71.49% \pm 0.41	47.23% \pm 1.17	69.63% \pm 0.39	45.22% \pm 0.98
Threshold conf	70.69% \pm 0.54	46.83% \pm 0.95	68.81% \pm 0.45	44.73% \pm 0.8
TempScaled AvgPred	71.96% \pm 0.38	48.27% \pm 0.96	70.18% \pm 0.28	45.85% \pm 0.81
TempScaled WeightedAvg	71.93% \pm 0.4	48.18% \pm 1.04	70.14% \pm 0.28	45.81% \pm 0.82
Concatenate + FC layers	70.94% \pm 0.37	49.64% \pm 0.54	68.95% \pm 0.28	46.17% \pm 0.5
WeightedLogitsComb	72.22% \pm 0.48	51.15% \pm 0.94	70.52% \pm 0.22	48.27% \pm 0.42
Best - WeightedLogitsComb		51.15% \pm 0.94		48.27% \pm 0.42
Oracle	97.69% \pm 2.82	56.14% \pm 0.93	75.84% \pm 0.24	53.27% \pm 1.01
FULL \times 2 Best - WLogitsComb		51.18% \pm 0.28		48.54% \pm 0.43
FG _C \times 2 Best - WLogitsComb		49.88% \pm 0.19		47.24% \pm 0.85

Table 9. FungiTastic results. Best corresponds to the best performing fusion on the validation set. Oracle prediction is correct if at least one of the fusion input’s prediction is correct.

Dataset	Val acc	Test acc	Test Ad acc	Test Ct acc
FULL	98.25% \pm 0.15	97.33% \pm 0.13	81.33% \pm 1.01	90.51% \pm 0.9
FG _C	98.18% \pm 0.18	97.79% \pm 0.32	85.93% \pm 1.31	90.1% \pm 1.81
BG _S	98.4% \pm 0.06	97.84% \pm 0.55	79.73% \pm 1.86	73.94% \pm 2.71
FG _C \oplus BG _S				
Max conf	98.75% \pm 0.09	98.77% \pm 0.22	90.0% \pm 0.8	91.11% \pm 3.38
Max scaled conf	98.84% \pm 0.04	98.88% \pm 0.31	89.91% \pm 0.48	91.31% \pm 2.63
Threshold conf	98.27% \pm 0.15	98.11% \pm 0.24	86.99% \pm 0.8	90.91% \pm 1.01
TempScaled AvgPred	98.85% \pm 0.05	98.91% \pm 0.29	90.44% \pm 0.86	91.31% \pm 1.53
TempScaled WeightedAvg	98.74% \pm 0.12	98.64% \pm 0.36	87.35% \pm 2.33	85.86% \pm 5.76
Concatenate + FC layers	98.94% \pm 0.02	98.99% \pm 0.2	90.0% \pm 1.31	92.12% \pm 1.32
WeightedLogitsComb	98.85% \pm 0.14	98.93% \pm 0.33	90.44% \pm 0.4	90.51% \pm 1.69
Best - Concat+ FC	98.94% \pm 0.02	98.99% \pm 0.2	90.0% \pm 1.31	92.12% \pm 1.32
Oracle	99.36% \pm 0.08	99.36% \pm 0.11	94.07% \pm 1.2	96.77% \pm 1.94
FG _C \oplus FULL				
Max conf	98.69% \pm 0.1	98.72% \pm 0.15	89.12% \pm 1.2	90.1% \pm 1.32
Max scaled conf	98.82% \pm 0.18	98.8% \pm 0.16	89.12% \pm 1.35	90.71% \pm 0.85
Threshold conf	98.26% \pm 0.15	98.11% \pm 0.3	87.17% \pm 0.54	89.9% \pm 1.24
TempScaled AvgPred	98.84% \pm 0.16	98.96% \pm 0.15	89.38% \pm 1.08	90.91% \pm 1.01
TempScaled WeightedAvg	98.74% \pm 0.07	98.61% \pm 0.31	87.96% \pm 0.58	90.91% \pm 1.01
Concatenate + FC layers	98.85% \pm 0.06	98.85% \pm 0.15	88.76% \pm 1.27	90.1% \pm 1.11
WeightedLogitsComb	98.82% \pm 0.05	99.01% \pm 0.28	89.38% \pm 1.25	90.71% \pm 0.85
Best - Concat+ FC	98.85% \pm 0.06	98.85% \pm 0.15	88.76% \pm 1.27	90.1% \pm 1.11
Oracle	99.32% \pm 0.05	99.47% \pm 0.09	92.57% \pm 0.48	92.12% \pm 1.11
FULL \times 2 Best - TempScaled WAvg	98.45% \pm 0.2	97.51% \pm 0.2	82.89% \pm 0.26	90.91% \pm 1.01
FG _C \times 2 Best - TempScaled WAvg	98.52% \pm 0.18	97.91% \pm 0.28	86.58% \pm 2.55	89.9% \pm 1.01

Table 10. HardImageNet results using OWLv2 generated masks using GT prompts. Best corresponds to the best performing fusion on the validation set. Oracle prediction is correct if at least one of the fusion input’s prediction is correct.

Dataset	Val acc	Test acc	Test LT acc	Test CT acc
FULL	98.25% \pm 0.15	97.33% \pm 0.13	81.33% \pm 1.01	90.51% \pm 0.9
FG _C	98.19% \pm 0.13	97.63% \pm 0.3	87.08% \pm 1.34	94.55% \pm 1.15
FG _M	95.6% \pm 0.22	95.39% \pm 1.15	85.4% \pm 1.77	95.56% \pm 1.53
BG _S	97.5% \pm 0.1	95.01% \pm 0.2	78.94% \pm 1.52	67.88% \pm 3.53
BG _B	94.02% \pm 0.31	91.76% \pm 0.49	56.64% \pm 2.1	24.24% \pm 2.77
FG _C \oplus BG _S				
Max conf	98.89% \pm 0.16	98.29% \pm 0.2	88.58% \pm 1.01	90.91% \pm 2.26
Max scaled conf	99.0% \pm 0.16	98.37% \pm 0.26	88.23% \pm 0.92	90.51% \pm 3.16
Threshold conf	98.26% \pm 0.1	97.63% \pm 0.37	87.7% \pm 1.75	94.14% \pm 1.11
TempScaled AvgPred	99.06% \pm 0.2	98.35% \pm 0.26	88.5% \pm 1.04	91.11% \pm 3.15
TempScaled WeightedAvg	98.82% \pm 0.25	98.16% \pm 0.2	88.05% \pm 1.68	90.51% \pm 4.66
Concatenate + FC layers	99.08% \pm 0.23	98.35% \pm 0.12	89.2% \pm 1.31	90.1% \pm 2.52
WeightedLogitsComb	99.13% \pm 0.19	98.45% \pm 0.18	89.56% \pm 1.35	90.3% \pm 2.91
Best - WeightedLogitsComb	99.13% \pm 0.19	98.45% \pm 0.18	89.56% \pm 1.35	90.3% \pm 2.91
Oracle	99.46% \pm 0.18	99.23% \pm 0.15	93.27% \pm 0.48	95.56% \pm 1.83
FG _C \oplus FULL				
Max conf	98.8% \pm 0.14	98.27% \pm 0.35	88.76% \pm 0.92	93.54% \pm 2.63
Max scaled conf	98.87% \pm 0.18	98.4% \pm 0.34	88.85% \pm 0.79	93.54% \pm 2.91
Threshold conf	98.26% \pm 0.13	97.63% \pm 0.37	88.14% \pm 1.45	94.75% \pm 1.5
TempScaled AvgPred	98.88% \pm 0.22	98.48% \pm 0.24	89.12% \pm 0.92	93.33% \pm 2.91
TempScaled WeightedAvg	98.81% \pm 0.14	98.29% \pm 0.22	88.76% \pm 0.67	93.33% \pm 2.73
Concatenate + FC layers	99.01% \pm 0.14	98.48% \pm 0.24	88.94% \pm 0.83	93.13% \pm 1.94
WeightedLogitsComb	99.0% \pm 0.14	98.48% \pm 0.2	89.65% \pm 0.86	93.13% \pm 2.41
Best - Concat+ FC	99.01% \pm 0.14	98.48% \pm 0.24	88.94% \pm 0.83	93.13% \pm 1.94
Oracle	99.46% \pm 0.1	99.36% \pm 0.26	93.27% \pm 0.58	96.16% \pm 1.94
FULL \times 2 Best - TempScaled WAvg	98.45% \pm 0.2	97.51% \pm 0.2	82.89% \pm 0.26	90.91% \pm 1.01
FG _C \times 2 Best - Concat + FC	98.43% \pm 0.09	97.96% \pm 0.34	87.17% \pm 0.77	94.95% \pm 1.01

Table 11. HardImageNet results using coarse ground truth masks provided by the original dataset authors. Best corresponds to the best performing fusion on the validation set. Oracle prediction is correct if at least one of the fusion input’s prediction is correct.

Dataset	Train acc	Val acc	Test acc
FULL	98.77% \pm 1.01	90.01% \pm 0.42	90.28% \pm 0.32
FG _C	97.28% \pm 1.56	90.89% \pm 0.36	91.25% \pm 0.25
FG _M	97.24% \pm 1.68	89.2% \pm 0.41	89.17% \pm 0.35
BG _S	97.36% \pm 2.53	51.8% \pm 0.74	51.34% \pm 0.94
BG _B	96.99% \pm 2.72	8.0% \pm 1.12	7.76% \pm 1.46
FG _C \oplus BG _S			
Max conf	98.75% \pm 1.27	83.54% \pm 4.1	83.78% \pm 4.07
Max scaled conf	98.27% \pm 1.29	89.98% \pm 0.35	90.51% \pm 0.25
Threshold conf	97.58% \pm 1.46	90.59% \pm 0.33	90.94% \pm 0.21
TempScaled AvgPred	98.46% \pm 1.16	90.0% \pm 0.28	90.59% \pm 0.27
TempScaled WeightedAvg	97.45% \pm 1.53	90.89% \pm 0.42	91.27% \pm 0.29
Concatenate + FC layers	99.65% \pm 0.31	80.16% \pm 4.54	79.77% \pm 4.88
WeightedLogitsComb	99.07% \pm 0.83	87.29% \pm 2.09	87.21% \pm 2.1
Best - TempScaled WAvG		90.89% \pm 0.42	91.27% \pm 0.29
Oracle	99.48% \pm 0.58	92.79% \pm 0.31	93.29% \pm 0.21
FG _C \oplus FULL			
Max conf	98.76% \pm 1.04	91.18% \pm 0.54	91.69% \pm 0.62
Max scaled conf	98.64% \pm 0.88	91.43% \pm 0.35	92.16% \pm 0.22
Threshold conf	97.56% \pm 1.38	91.08% \pm 0.27	91.66% \pm 0.25
TempScaled AvgPred	98.67% \pm 0.88	91.41% \pm 0.33	92.15% \pm 0.23
TempScaled WeightedAvg	98.27% \pm 1.07	91.34% \pm 0.41	92.01% \pm 0.33
Concatenate + FC layers	99.2% \pm 0.66	91.37% \pm 0.32	91.63% \pm 0.44
WeightedLogitsComb	98.85% \pm 0.94	91.34% \pm 0.26	92.06% \pm 0.31
Best - Max scaled conf		91.43% \pm 0.35	92.16% \pm 0.22
Oracle	99.17% \pm 0.73	93.9% \pm 0.4	94.47% \pm 0.3
FULL \times 2 Best - Concat + FC		91.07% \pm 0.23	91.13% \pm 0.17
FG _C \times 2 Best - Concat + FC		91.65% \pm 0.42	91.9% \pm 0.03

Table 12. Stanford dogs. Best corresponds to the best performing fusion on the validation set. Oracle prediction is correct if at least one of the fusion input’s prediction is correct.

Dataset	Test acc	Test clean
FULL	82.35	92.01
FG _C	85.56	91.99
BG _S	73.24	81.28
<hr/>		
FG _C \oplus BG _S		
<hr/>		
Max conf	86.39	93.02
Max scaled conf	86.57	93.19
Threshold conf	86.57	93.18
TempScaled AvgPred	86.77	93.32
TempScaled WeightedAvg	86.93	93.33
Concatenate + FC layers	86.38	92.76
WeightedLogitsComb	87.13	93.30
Best - WeightedLogitsComb	87.13	93.30
<hr/>		
FG _C \oplus FULL		
<hr/>		
Max conf	86.22	93.50
Max scaled conf	86.38	93.48
Threshold conf	86.38	93.48
TempScaled AvgPred	86.58	93.60
TempScaled WeightedAvg	86.41	93.57
Concatenate + FC layers	86.00	92.77
WeightedLogitsComb	87.04	93.76
Best - WeightedLogitsComb	87.04	93.76

Table 13. ImageNet results using OWLv2 generated masks using GT prompts. Best corresponds to the best performing fusion on the validation set.

Dataset	Train acc	Val acc	Test acc
FULL	100.0% \pm 0.01	100.0% \pm 0.0	43.2% \pm 9.74
FG _C	99.96% \pm 0.07	99.91% \pm 0.05	91.31% \pm 3.45
FG _M	99.96% \pm 0.06	99.7% \pm 0.08	95.28% \pm 1.47
BG _S	100.0% \pm 0.0	99.83% \pm 0.04	2.62% \pm 0.8
BG _B	99.94% \pm 0.06	99.18% \pm 0.12	0.18% \pm 0.08
FG _C \oplus BG _S			
Max conf	100.0% \pm 0.0	99.98% \pm 0.02	25.9% \pm 20.5
Max scaled conf	100.0% \pm 0.0	100.0% \pm 0.0	66.15% \pm 28.27
Threshold conf	99.96% \pm 0.07	99.91% \pm 0.05	91.25% \pm 3.47
TempScaled AvgPred	100.0% \pm 0.0	100.0% \pm 0.0	65.81% \pm 27.59
TempScaled WeightedAvg	100.0% \pm 0.0	99.99% \pm 0.02	70.39% \pm 38.02
Concatenate + FC layers	100.0% \pm 0.0	99.97% \pm 0.04	49.68% \pm 11.85
WeightedLogitsComb	100.0% \pm 0.0	99.98% \pm 0.02	27.71% \pm 18.67
Best		100.0% \pm 0.0	65.81-66.15%
Oracle	100.0% \pm 0.0	100.0% \pm 0.0	91.32% \pm 3.45
FG _C \oplus FULL			
Max conf	100.0% \pm 0.0	100.0% \pm 0.0	76.66% \pm 7.28
Max scaled conf	100.0% \pm 0.0	100.0% \pm 0.0	51.86% \pm 16.57
Threshold conf	99.96% \pm 0.07	99.91% \pm 0.05	91.26% \pm 3.47
TempScaled AvgPred	100.0% \pm 0.0	100.0% \pm 0.0	52.02% \pm 16.71
TempScaled WeightedAvg	100.0% \pm 0.01	100.0% \pm 0.0	43.2% \pm 9.74
Concatenate + FC layers	100.0% \pm 0.0	100.0% \pm 0.0	68.41% \pm 14.15
WeightedLogitsComb	100.0% \pm 0.0	100.0% \pm 0.0	76.95% \pm 6.83
Best		100.0% \pm 0.0	43.06-76.95%
Oracle	100.0% \pm 0.0	100.0% \pm 0.0	91.57% \pm 3.47
FULL \times 2 Best		100.0% \pm 0.0	40-45%
FG _C \times 2 Best - Concat + FC		100.0% \pm 0.0	94.62% \pm 1.65

Table 14. Result of ConvNeXt models on the Spawrious dataset. Best corresponds to the best performing fusion on the validation set. Oracle prediction is correct if at least one of the fusion input’s prediction is correct.

Dataset	Train acc	Val acc	Test acc
Timm Resnet50			
FULL	99.76% \pm 0.06	99.3% \pm 0.19	87.38% \pm 0.71
FG _C undistorted	99.46% \pm 0.05	99.12% \pm 0.1	95.02% \pm 1.04
FG _C distorted	99.06% \pm 0.08	98.34% \pm 0.22	94.26% \pm 0.95
FG _M distorted	98.81% \pm 0.03	98.36% \pm 0.11	94.83% \pm 0.29
FG _M undistorted	99.06% \pm 0.19	98.69% \pm 0.17	95.42% \pm 0.52
BG _S	98.66% \pm 0.12	97.54% \pm 0.12	24.26% \pm 4.39
BG _B	95.67% \pm 0.13	94.89% \pm 0.27	0.72% \pm 0.14
FG \oplus_R BG	99.79% \pm 0.05	99.55% \pm 0.04	91.37% \pm 0.8
Torchvision Resnet50			
FULL	100.0% \pm 0.0	99.85% \pm 0.04	71.35% \pm 3.72
FG _C undistorted	100.0% \pm 0.0	99.83% \pm 0.05	95.0% \pm 0.63
FG _C distorted	99.99% \pm 0.01	99.61% \pm 0.08	94.97% \pm 0.44
FG _M distorted	100.0% \pm 0.0	99.42% \pm 0.08	95.22% \pm 0.12
FG _M undistorted	100.0% \pm 0.0	99.58% \pm 0.05	95.59% \pm 0.25
BG _S	100.0% \pm 0.0	99.21% \pm 0.16	8.9% \pm 1.38
BG _B	99.76% \pm 0.3	96.94% \pm 0.08	0.36% \pm 0.03
FG \oplus_R BG	100.0% \pm 0.0	99.91% \pm 0.06	86.78% \pm 3.95

Table 15. Spawrious. Resnet50 models, same architecture, with two different initializations (timm and torchvision). The Timm pretrained checkpoints are significantly more robust.